SURFACE VEHICLE RECOMMENDED PRACTICE

J3116™ JAN2023

Issued 2017-06
Reaffirmed 2023-01

Superseding J3116 JUN2017

Active Safety Pedestrian Test Mannequin Recommendation

RATIONALE

Improving pedestrian safety is one of the major goals for active safety systems. As more active safety systems, especially the automatic emergency braking systems, are introduced to the market, a standard surrogate pedestrian target is needed for automotive industries to test and evaluate the PCS systems. SAE International created an Active Safety Pedestrian Test Mannequin Task Force under the Active Safety Systems Standards Committee to study this topic and to recommend a mannequin standard. All members of the task force are from industry, government, and academia and many members had experience in using and/or developing pedestrian mannequins and testing them. The task force gathered information of all mannequins known to the committee members and analyzed the state of the art features of these mannequins. The goal of the Pedestrian Test Mannequin Task Force is to develop standard specifications/requirements for pedestrian test mannequins (one adult and one child) that are representative of real pedestrians to the sensors used in forward looking pedestrian detection systems and can be used for performance assessment of such in-vehicle systems (including warning and/or braking) in real world test scenarios/conditions. This document is the result of committee study and recommendation.

SAE J3116 has been reaffirmed to comply with the SAE Five-Year Review policy.

INTRODUCTION

Improving pedestrian safety is one of the major goals for active safety systems. As more active safety systems, especially the automatic emergency braking systems, are introduced to the market, a standard surrogate pedestrian target is needed for automotive industries to test and evaluate the PCS (Pre-crash systems). SAE International created an Active Safety Pedestrian Test Mannequin Task Force under the Active Safety Systems Standards Committee to study this topic and to recommend a mannequin standard for frontal pedestrian detection systems. All members of the task force are from industry, government, and academia and many members had experience in using and/or developing pedestrian mannequins and testing them. The task force gathered information of all mannequins known to the committee members and analyzed the state of the art features of these mannequins [1, 2]. This document is the result of committee study and recommendation.

The task force reviewed a similar standard created by ISO [3] as a group including feedback from members who are familiar with ISO activity. The task force understood that this ISO test mannequin standard was created based on European data and mannequin specification is for side view and front view. The SAE workgroup is for developing a target based on US specific data and US population. This SAE mannequin specification is also for 360° views.

TO PLACE A DOCUMENT ORDER: Tel: 877-606-7323 (inside USA and Canada)
Tel: +1 724-776-4970 (outside USA)
Fax: 724-776-0790
Email: CustomerService@sae.org
SAE WEB ADDRESS: http://www.sae.org

For more information on this standard, visit
https://www.sae.org/standards/content/J3116_202301/

TABLE OF CONTENTS

1. SCOPE

The goal of the Pedestrian Test Mannequin Task Force is to develop standard specifications/requirements for pedestrian test mannequins (1 adult and 1 child) that are representative of real pedestrians to the sensors used in Pedestrian Detection systems and can be used for performance assessment of such in-vehicle systems (including warning and/or braking) in real world test scenarios/conditions. This version of the document only includes the pedestrian mannequin for vision, Lidar, and/or 76 to 78 GHz radar based Pedestrian Pre-collision systems.

2. REFERENCES

[1] Qiang Yi, Stanley Chien, Jason Brink, David Good, Chi-Chih Chen, Yaobin Chen, Lingxi Li, and Rini Sherony, “Mannequin Development for Pedestrian Pre-Collision System Evaluation,” 2014 Intelligent Transportation Systems Conference, Oct. 2014, Qingdao China.

[2] http://www.4activesystems.at/en.

[3] ISO/DIS 19206-2, Road vehicles – test devices for target vehicles, volnerable road users and other objects, for assessment of active safety functions – Part 2: Requirements for pedestrian targets.

[4] M. Yanagisawa, E. Swanson, and W.G. Najm, “Target Crashes and Safety Benefits Estimation Methodology for Pedestrian Crash Avoidance/Mitigation Systems,” Washington, DC: National Highway Traffic Safety Administration, 2014.

[5] MakeHuman – Open source tool to make human characters, http://www.makehuman.org/index.php.

[6] CDC, http://www.cdc.gov/nchs/data/nhsr/nhsr010.pdf.

[7] Anthropometric Reference Data for Children and Adults: United States, 2011-2014. http://www.cdc.gov/nchs/data/series/sr_03/sr03_039.pdf.

[8] Open Design Lab at PSU, http://openlab.psu.edu/tools/explorer.php.

[9] 2012 Anthropometric Survey of US Army Personnel: Methods and Summary Statics, http://www.dtic.mil/cgi-bin/GetTRDoc?AD=ADA611869.

[10] Anthropometric Reference Data for Children and Adults: United States, 1988-1994, http://www.cdc.gov/nchs/data/series/sr_11/sr11_249.pdf.

[11] N036 ISO WD 19206-2, Active Safety Targets Pedestrian Targets, Rev. 2015-11-20.

[12] Sherony, R., Tian, R., Chien, S., Fu, L., Chen, Y., and Takahashi, H., “Pedestrian/Bicyclist Limb Motion Analysis from 110-Car TASI Video Data for Autonomous Emergency Braking Testing Surrogate Development,” Presentation at SAE International 2016 World Congress, Apr. 2016.

[13] Sherony, R., Tian, R., Chien, S., Fu, L., Chen, Y., and Takahashi, H., “Pedestrian/Bicyclist Limb Motion Analysis from 110-Car TASI Video Data for Automatic Emergency Braking Testing Surrogate Development,” Presentation at SAE International 2016 World Congress, Apr. 2016.

[14] Tommy Oberg, Alek Karsznia, and Kurt Oberg, “Joint Angle Parameters in Gait: Reference Data for Normal Subjects, 10-79 Years of Age,” *Journal of Rehabilitation Research and Development* 31, no. 1 (Aug. 1994): 199-213.

[15] Richard W. Bohannon, “Comfortable and Maximum Walking Speed Of Adults Aged 20-79 Years: Reference Values and Determinants,” Age and Ageing, 1997:26: pp. 15-19.

[16] Stanley Chien, Libo Dong, Qiang Yi, Yaobin Chen, Rini Sherony, and Hiroyuki Takahashi, “Joint Motion Pattern of Limb Moving Mannequins for Active Safety Vehicle Tests,” 2013 ESV Conference, Paper Number: 13-0219, Nagoya, Japan, Jun. 2013.

[17] Tom F. Novacheck, "The Biomechanics of Running," *Gait and Posture* 7 (1998): 77-95. http://www.elitetrack.com/article_files/biomechanicsofrunning.pdf.

[18] Libo Dong, Stanley Chien, Kai Yang, Yaobin Chen, David Good, and Rini Sherony, "Determination of Pedestrian Mannequin Clothing Color for the Evaluation of Image Recognition Performance of Pedestrian Pre-Collision Systems," 2015 ESV Conference, Gothenburg Sweden, Jun. 2015.

[19] John A. Jacquez, John Huss, Wayne McKeehan, James M. Dimitroff, and Hans F. Kuppenheim, "Spectral Reflectance of Human Skin in the Region 0.7–2.6 μ," *Journal of Applied Physiology* 8, no. 3 (Nov. 1, 1955): 297-299, http://jap.physiology.org/content/8/3/297.full-text.pdf+html.

[20] Catherine C. Cooksey, Benjamin K. Tsai, and David W. Allen, "A Collection and Statistical Analysis of Skin Reflectance Signatures for Inherent Variability over the 250 nm to 2500 nm Spectral Range," Proc. of SPIE Vol. 9082, 908206 2014, http://www.nist.gov/customcf/get_pdf.cfm?pub_id=916057.

[21] Terence Haran, and Stanley Chien, "Infrared Reflectivity of Pedestrian Mannequin for Autonomous Emergency Braking Testing," 2016 IEEE ITSC Conference, Nov. 2016, Rio, Brazil.

[22] Falconer, D.G., "Extrapolation of Near-field RCS Measurements to the Far Zone," *IEEE Transactions on Antennas and Propagation* 36, no.6 (Jun. 1988): 822, 829. doi:10.1109/8.1184.

[23] European Commission DG RTD Seventh Framework Pogramme Theme 7 Transport–SST SST.2011.Rtd-1 GA No. 285106.

[24] M. Chen, C.-C. Chen, S. Y.-P. Chien, and R. Sherony, "Artificial Skin for 76-77 GHz Radar Mannequins," *IEEE Trans. on Antennas and Propagation* 62, no. 11 (Nov. 2014): 5671-5679.

[25] Euro NCAP AEB VRU Test Protocol v1.0.1, http://euroncap.blob.core.windows.net/media/21509/euro-ncap-aeb-vru-test-protocol-v101.pdf.

[26] D. Belgiovane, C.-C. Chen, M. Chen, S.Y.P. Chien, and R. Sherony, "77 GHz Radar Scattering Properties of Pedestrians", IEEE Radar Conference, 735-738, May 2014.

[27] M. Chen, C.-C. Chen, S. Y.-P. Chien, and R. Sherony, "Artificial Skin for 76-77 GHz Radar Mannequins," *IEEE Transactions on Antennas and Propagation* 62, no. 11 (Nov. 2014): 5671-5679.

[28] Falconer, D.G., "Extrapolation of Near-field RCS Measurements to the Far Zone," *IEEE Transactions on Antennas and Propagation* 36, no. 6 (Jun. 1988): 822, 829. doi: 10.1109/8.1184.

[29] B. R. Mahafza, Radar systems analysis and design using MATLAB. Chapman and Hall/CRC, 2000.

[30] M. Chen, M. Kuloglu and C.-C. Chen, "Numerical Study of Pedestrian RCS at 76-77 GHz," IEEE Antennas and Propagation Society International Symposium, July 2013.

[31] "Human Skin Dielectric Property" http://niremf.ifac.cnr.it/tissprop/.

[32] M. Chen, C.-C. Chen, S. Y.-P. Chien, R. Sherony, "Artificial Skin for 76-77 GHz Radar Mannequins," *IEEE Transactions on Antennas and Propagation* 62, no. 11 (Nov. 2014): 5671-5679. US Patent 9,263,800.

[33] B. R. Mahafza, Radar systems analysis and design using MATLAB. Chapman and Hall/CRC, 2000.

[34] Falconer, D.G., "Extrapolation of Near-field RCS Measurements to the Far Zone," *IEEE Transactions on Antennas and Propagation* 36, no. 6 (Jun. 1988): 822,829. doi: 10.1109/8.1184.

3. TERMS AND DEFINITIONS

ACTIVE SAFETY SYSTEM: Active safety systems are vehicle safety systems that sense and monitor conditions inside and outside the vehicle, identify perceived present and potential dangers to the vehicle, occupants, and other roadway users, and then automatically react to help avoid or mitigate crashes via various methods including alerts, vehicle system adjustments, and active control of the vehicle motion subsystems (brakes, throttle, suspension, etc.).AEB: Automatic emergency braking (AEB) systems detect an impending forward crash with another vehicle in time to avoid or mitigate the crash. These systems first alert the driver to take corrective action to avoid the crash. If the driver's response is not sufficient to avoid the crash, the AEB system may automatically apply the brakes to assist in preventing or reducing the severity of a crash (https://www.safercar.gov/Vehicle-Shoppers/Safety-Technology/AEB/aeb).

ANECHOIC: Free from echo (like an anechoic chamber).

ARTICULATION: Arm and leg rotation on a mannequin similar to a real walking human.

CADENCE: The rate at which a person walks, expressed in steps per minute.

CUBIC Spline Fitting: Gait planning method based on the function $f_i(x) = a_i + b_i x + c_i x^2 + d_i x^3$.

GAIT: The pattern of movement of the limbs during walking.

INFRARED: Have a wavelength just greater than that of the red end of the visible light spectrum but less than that of microwaves. Infrared radiation has a wavelength from about 800 nm to 1 mm, and is emitted particularly by heated objects. Passive infrared systems can detect any heat emitted by warm objects. Active systems use an infrared light source built into the car to illuminate the road ahead with light that is invisible to humans.

LIDAR: A technology that measures distance by illuminating a target with a laser light.

MICRO DOPPLER: Mechanical vibrations/rotations/movements of a target or structures on the target may induce additional frequency modulations on the returned radar signal that generate sidebands about the target's body return Doppler frequency. These frequency modulations are called the micro-Doppler effect.

MONO CAMERA: Monocular, i.e., single camera.

NATURALISTIC DRIVING STUDY (NDS): A study to provide insight into driver behavior during every day trips by recording details of the driver, the vehicle and the surroundings through unobtrusive data gathering equipment and without experimental control (http://www.udrive.eu/index.php/about-udrive/what-is-naturalistic-driving).

4. SYMBOLS AND ABBREVIATIONS

AEB	Automatic Emergency Braking
AsPeCSS	Assessment methodologies for forward-looking integrated pedestrian safety systems
BMI	Body Mass Index
FARS	Fatality Analysis Reporting System
GES	General Estimate System
IIHS	Insurance Institute for Highway Safety
Lidar	Light Detection and Ranging
NHANES	National Health and Nutrition Examination Survey
NHTSA	National Highway Traffic Safety Administration
PAEB	Pedestrian Automatic Emergency Braking

PCS Pre-Crash System

Radar Radio Detection and Ranging

RCS Radar Cross Section

TASI Transportation Active Safety Institute

5. PEDESTRIAN TARGET SPECIFICATIONS

The pedestrian targets should provide sufficient details of the pedestrian characteristics to satisfy the need of all state-of-the-art PCS sensors and anticipated potential new PCS sensing technologies. Following table shows the pedestrian characteristics that have potential effect to the sensing outcome. They should be considered in the pedestrian target specifications.

Table 1 - Mannequin characteristics versus PCS sensors

SENSOR TYPE	MANNEQUIN CHARACTERISTICS				
	SIZE	ARTICULATION	RCS	VIEWING ANGLE	CLOTHING COLOR
MONO CAMERA	X	X		X	X
STEREO CAMERA	X	X		X	X
76-78 GHZ RADAR	X	X	X	X	
MICRO DOPPLER	X	X	X	X	
LIDAR	X			X	X
INFRARED	X	X		X	X

5.1 Viewing Angles

Although most current PCS testing requires the back view and the 90° side view of the pedestrian target, the PCS are frequently exposed to pedestrians from different angles during naturalistic driving. Figure 1 shows that PCS sensors can detect the mannequin from different angles even if only pedestrian crossing the road and moving along the road are tested. The shape differences of the human body may affect the pedestrian detection capability of cameras, radar and Lidar. The shape change leads to surface area change that affect the RCS (Figure 2). Therefore, it is essential that a standard mannequin target look like a real human from all PAEB sensors in 360° angles.

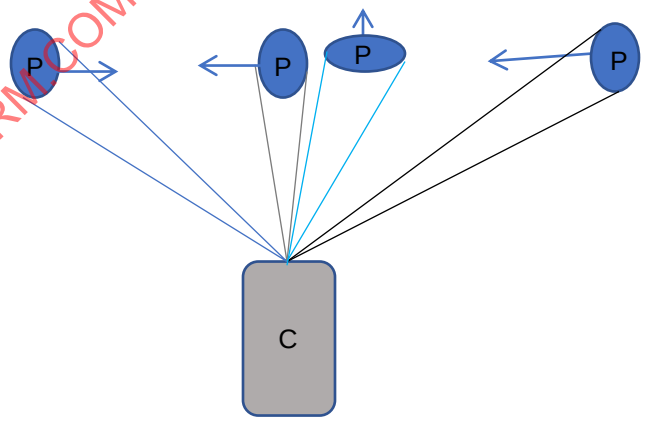

Figure 1 - Vehicle detects the pedestrian body from different angles when the pedestrian is crossing the road and along the road

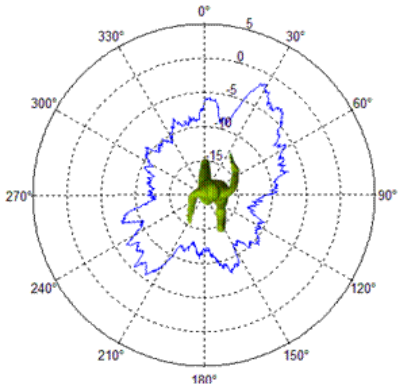

Figure 2 - Measured RCS data of a human subject (173 cm tall and weight 54.4 kg) at walking posture from 360° angles

5.2 Pedestrian Size

This document only specifies two mannequin sizes; adult and child. Historically, pedestrian characteristics have been drawn from similar studies of vehicle occupants. The 50th percentile male adult size (180 cm) and the 6 years old child size (120 cm) were used for safety tests of vehicle occupant. Similarly, NHTSA (National Highway Traffic Safety Administration), IIHS (Insurance Institute for Highway Safety), and AsPeCSS used the 50th percentile male adult size and the 6 years old child size as the sizes for pedestrian PCS test mannequins.

Since 180 cm is the 50th percentile of European male population and does not consider the female population, the committee decided to determine the mannequin height based on the pedestrian crash statistics in the United States and include both male and female population.

In the U.S., 30.1% of fatal pedestrian crash and 43% pedestrian injuries are female according to 2014 NHTSA data (e).

In the US, the 50th percentile height of male adults is 175.6 cm, and the 50th percentile height of female adults is 162.9 cm according to CDC data (http://www.cdc.gov/nchs/data/series/sr_03/sr03_039.pdf).

Therefore, the adult mannequin height is determined as 175.6 x 69.9% + 162.9 x 30.1% = 171.5 cm

According to NHTSA, children are defined as 14 and younger (https://crashstats.nhtsa.dot.gov/Api/Public/ViewPublication/812154).

The height of child mannequin size will be the average height of 6 years old boys and girls, which is 120.1 cm according to CDC's child growth chart (http://www.cdc.gov/nchs/data/series/sr_03/sr03_039.pdf). Since the number of children involved in frontal pedestrian crashes is small (5% of the pedestrian traffic fatalities were children from 2013 FARS Data, refer to NHTSA Report DOT HS 812 154), we did not calculate a weighted value of boys and girls similar to the above calculation for adult pedestrians. The back over child mannequin size can be referenced (we are not considering the mannequin for back over, just referencing how the child size was determined).

The anthropometry of the test mannequin is determined according to the values in http://www.cdc.gov/nchs/data/nhsr/nhsr010.pdf.

The measurements of the mannequin body parts are shown in Figure 3. The sizes of the adult and child are on the right two columns of Table 2 (without shoes).

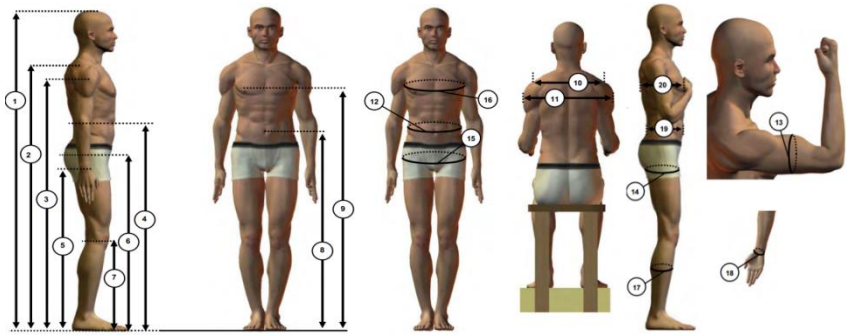

Figure 3 - Mannequin body parts model

Table 2 - Detailed fit-adult body dimensions

Index	Measurements	Description	Adult (mm)	Data Source
1	Stature	Head to toe height	1715	NHANES (2011-2014) [4]
3	Shoulder pivot height	Mid-shoulder cap to toe	1407	NHANES [5]
4	Elbow height	Elbow to toe	1084	NHANES
5	Wrist height	From wrist to toe	834	NHANES
6	Hip pivot/Buttocks height	Hip pivot to toe	912	NHANES
7	Knee pivot height	Knee pivot to toe	490	NHANES
10	Biacromial breadth	Distance between shoulders from the back but not including shoulder cap basically from armpit to armpit from the back	408	NHANES
11	Bideltoid breadth	Distance between shoulders from back	491	ANSUR 2012 [6]
16	Chest circumference	Around chest underneath armpits, chest circumference at axilla	1030	NHANES
12	Waist circumference	Measured around belly button	914	NHANES
15	Buttock circumference	Measured around hips	1062	NHANES
13	Upper arm (biceps) circumference	The circumference of the right upper arm around the flexed biceps	341	ANSUR 2012
14	Thigh circumference	The circumference of the right thigh at the gluteal furrow	621	ANSUR 2012
17	Calf circumference	The maximum horizontal circumference of the right calf	386	ANSUR 2012

Table 2 - Detailed fit-adult body dimensions (continued)

Index	Measurements	Description	Child 6 Years old (mm)	Data source
1	Stature	Head to toe height	1201	NHANES (2011-2014) [7]
3	Upper arm length		238	NHANES III [10]
6	Upper leg length		272	NHANES III
10	Biacromial breadth	Distance between shoulders from the back but not including shoulder cap basically from armpit to armpit from the back	262	NHANES III
12	Waist circumference	Measured around belly button	541	NHANES III
15	Buttock circumference	Measured around hips	595	NHANES III
13	Upper arm (biceps) circumference	The circumference of the right upper arm around the flexed biceps	184	NHANES III
14	Thigh circumference	The circumference of the right thigh at the gluteal furrow	328	NHANES III

5.3 Postures

The pedestrian target and any associated supporting devices should be able to achieve and maintain a torso inclination angle of up to 12° leaning forward. This torso inclination can be utilized to more accurately simulate the posture of a moving pedestrian (e.g., angled 5° for a walking adult and 12° for a running child [11]).

5.4 Articulation

The performance of many PCS sensors may be affected by articulation since it changes the apparent size and shape of the pedestrian. Figure 4 show the effect of articulation on the RCS measurement. The articulation is essential for the micro Doppler radar to detect the pedestrian. Therefore, articulation should be considered as one of the characteristics of the mannequin for standard PCS testing. For radar systems that utilize micro-Doppler as detection features, the arms and legs of the pedestrian mannequin for this purpose should have similar articulations and gait cycles as real walking or running pedestrians. Leg articulations have shown stronger micro Doppler response than arm articulation (see Figure A6). The legs and arms also need to be able to have proper RCS levels and patterns. Articulation of legs, therefore, is strongly recommended.

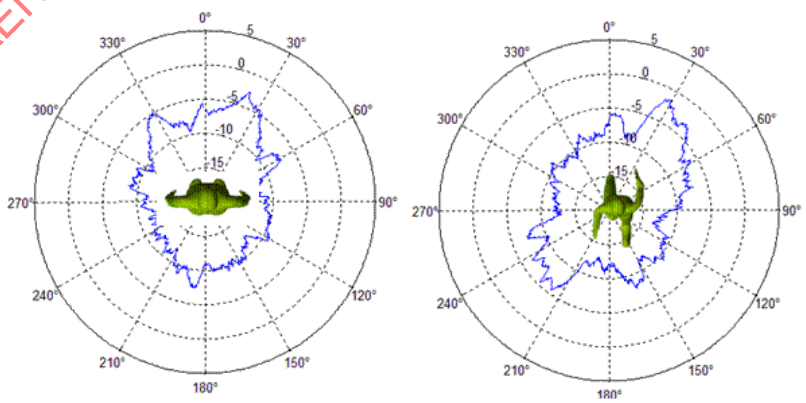

Figure 4 - Effect of articulation to RCS of a human subject (173 cm tall and weight 54.4 kg) at standing and walking posture from 360° angles

As shown in Figure 5, the RCS of legs is higher than the RCS of arms in general. The presence/absence of the arm can affect RCS significantly in some angles.

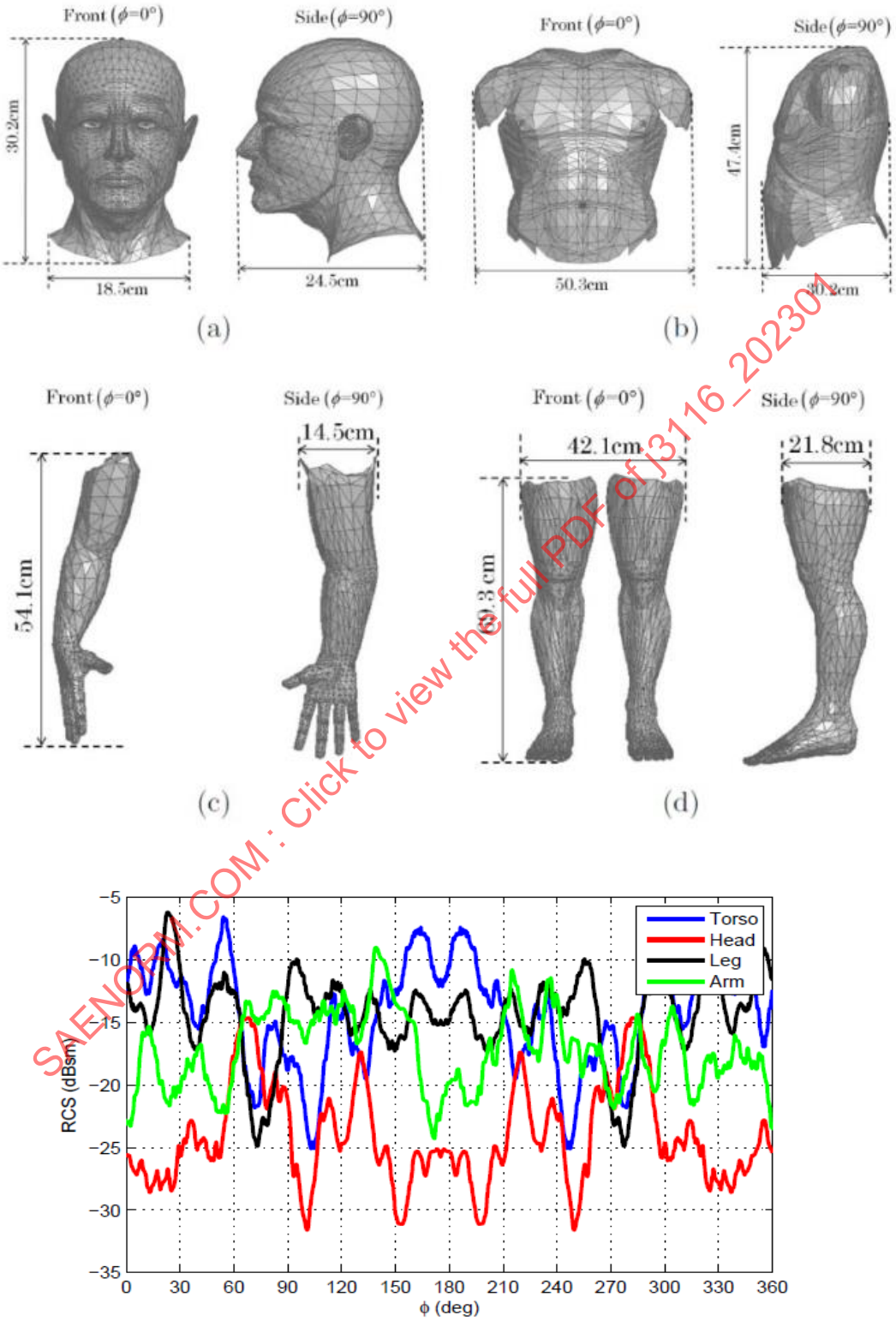

Figure 5 - Simulated 77 GHz scattering from different body parts

Since the committee is not aware of any active safety systems which use the neck or torso articulation information for pedestrian detection, the neck and torso articulation should not be required for the pedestrian target.

Naturalistic driving study concluded that about only 54% of pedestrians move one or both arms when crossing the street, therefore the articulation of arms is optional, however if implemented, the articulation of the arms should be consistent with natural human movement [12].

5.5 Gaiting

The articulation of the pedestrian target shall demonstrate leg motions consistent with the standard gait phases of the human. Heel contact initiates the beginning of the gait cycle and stance is followed by the swing phase. A complete gait cycle includes the stance-to-swing transition and should be used as the beginning and ending of the gait cycle. http://www.utdallas.edu/atec/midori/Handouts/walkingGraphs_files/gait.JPG .

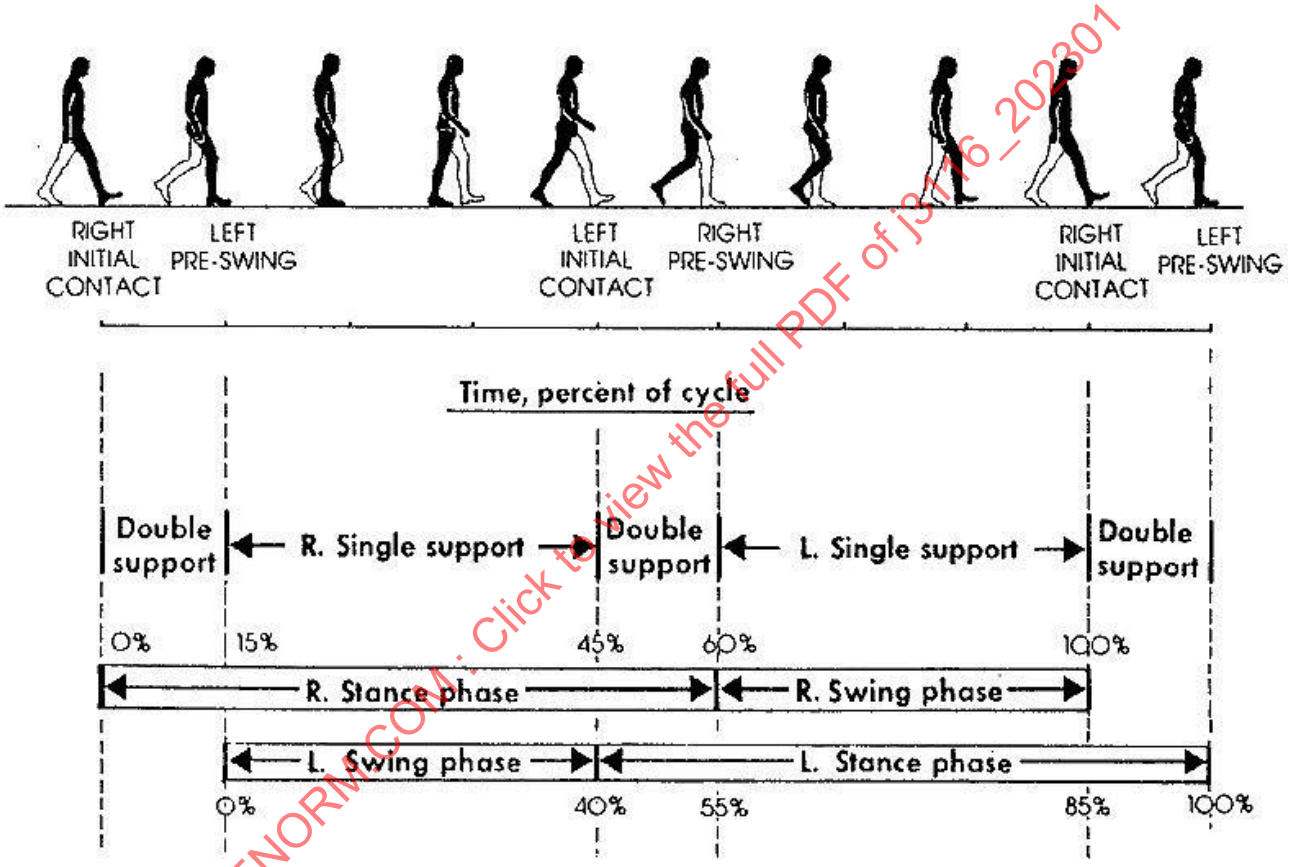

Figure 6 - Eight stage human gait description

Although the human gaits can be described in eight stages, there is no quantitative hip and knee joint angle profiles that represent the pedestrian population. Therefore, it does not provide sufficient information for mannequin joint motion implementation. A simplified four-stage gait description is used. The quantitative hip and knee joint angle profiles can be obtained in literature. Figure 7 depicts 4 postures of the legs in a walking gait cycle, 1 = heel contact, 2 = mid-stance, 3 = heel-off, 4 = mid swing which corresponds to stages 1, 3, 5, and 7 in Figure 6, respectively.

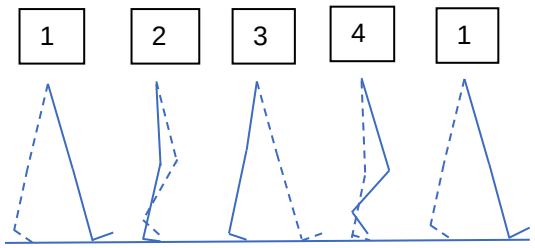

Figure 7 - Four stage human gait description used for mannequin articulation

5.5.1 Gait Step and Cadence

Based on the gait measurement of 493 people from age 10 to 79 in two studies from the U.S. and Sweden [14, 15], the step size (m) and step frequency (steps/second) are functions of motion speed (m/s) (see Figure 8). According to the data in [16], the step size (m) and step frequency (steps/second) with respect to running speed (m/s) are shown in Figure 9. Since the maximum pedestrian motion speed is 2.64 m/s, the limbs should be able to move at 3 steps/second or 1.5 Hz (2 steps equal 1 full gait cycle).

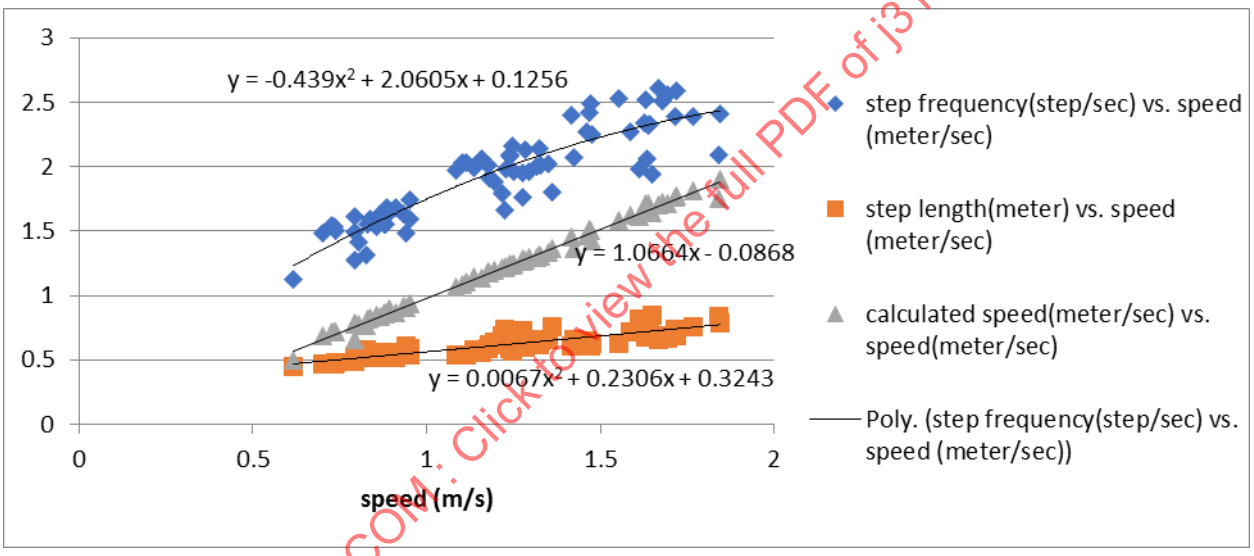

Figure 8 - Step size (m) and step frequency (steps/second) on vertical axes with respect to walking speed (m/s) on horizontal axis

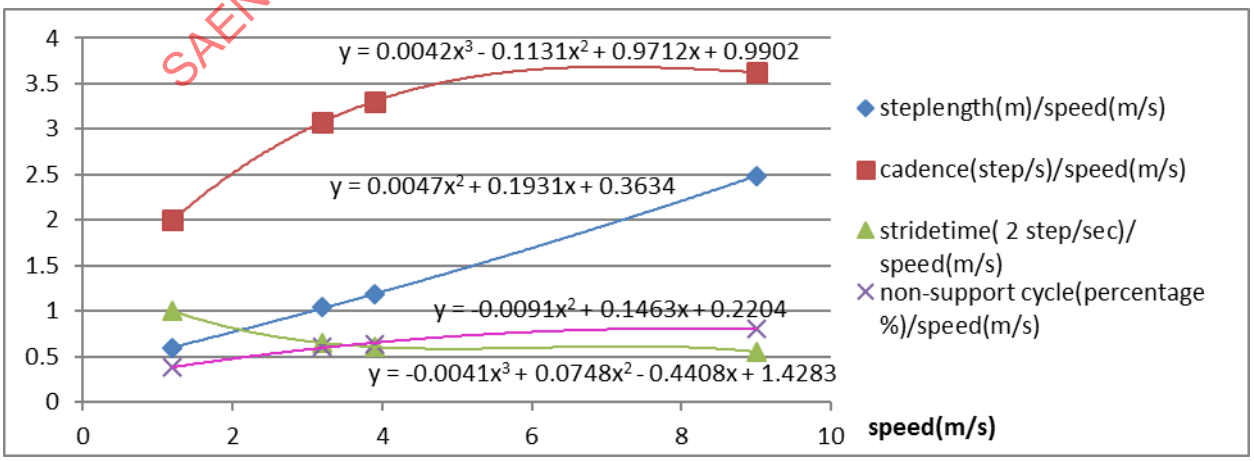

Figure 9 - Adult running step length (m) and step frequency (steps/second) versus running speed (m/s)

5.5.2 Extrema Joint Angles

Based on the research of [17], the extrema joint angles and gait timing of the extrema joint angles in terms of % cycles were obtained (see Table 3).

Table 3 - The summary of gait parameters calculation for adult mannequin

	Extrema angles (X: walking speed in cm/s)	Extrema at cycle percentage (X: walking speed in cm/s)
Hip Flexion/Extension (degrees)	Flexion - Extension: 27.8 + 016*X	Flexion: 0.5298*X2 - 8.3022*X + 103.87 Extension: 0.3272*X2 - 5.6556*X + 57.385
Knee Stance (degrees)	Flexion - Extension: 1.25 + 0.135*X	Flexion: 0.2116*X2 - 2.9312*X + 43.213 Extension : -1.0714*X2 + 5.4643*X + 5.9857
Knee Swing (degrees)	Flexion - Extension: 56.7+0.068*X	Flexion: -0.0994*X3 + 1.4069*X2 - 7.6479*X + 79.323 Extension : 0.2384*X2 - 2.5343*X + 100.53

5.5.3 Gait Planning

Cubic spline fitting method was used to generate the smooth and jerk-free joint motions. As example, Figures 10 and 11 shows the fitted curves and stick frames in one biped cycle of speed 1.2 m/s.

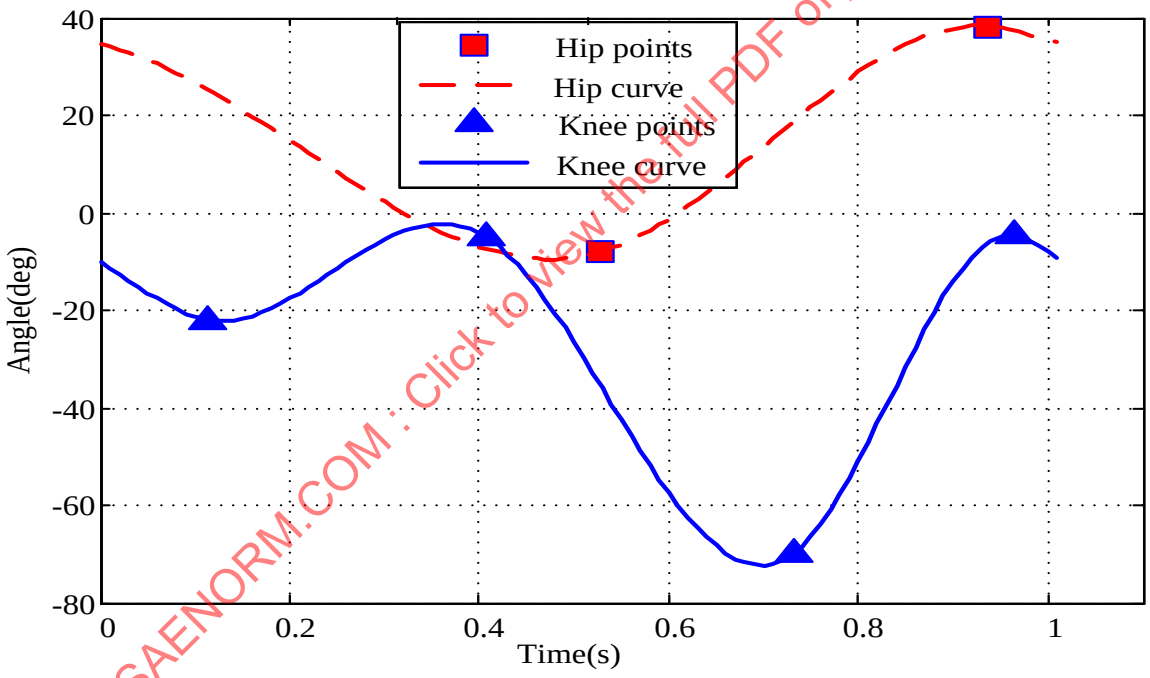

Figure 10 - Pivot points and fitted curve of one mannequin walking gait cycle

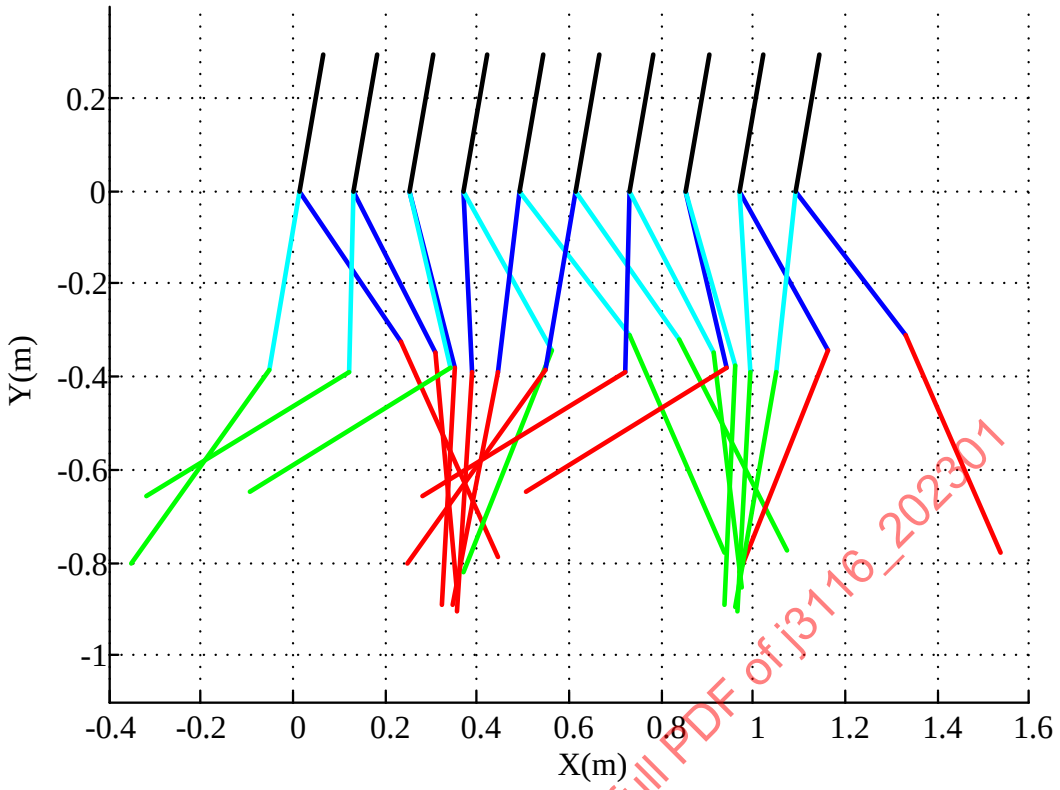

Figure 11 - Stick frames of mannequin legs in one cycle. Vertical line is 0° for the hip angle. Upper leg on the right of the verticle line is positive angle and on the left of the verticle line is the negative angle. The knee angle is 0 when the upper leg and lower leg are aligned.

5.6 Visual Characteristics of Head and Hands

The portions of the mannequins which are not covered by clothing should visually resemble a real human pedestrian. It is recognized that pedestrians will have various skin and hair colors and that sensing systems should be designed to detect all variations equally well. However, for purpose of this specification, the mannequins shall minimally include the following features:

- Human skin tone representative of the middle third of the Von Luschan chromatic scale (ranging between 10 and 27 on this scale).
- Brown or black simulated hair representative of the most common global hair colors (ranging between P and Y on the Fischer – Saller scale). The hair may simply be represented by an appropriately colored and shaped portion of the mannequin's outer covering.
- Facial features (eyes, nose, mouth, ears, etc.) are not typically utilized by current pedestrian detection system algorithms. Therefore, these features are not currently required for the pedestrian mannequins.

5.7 Clothing

Clothing is needed for the pedestrian target since it affects the appearance size and may affect the data processing of optical based sensors. Radar measurement shows that both summer and winter clothing have insignificant influences on the RCS return (Figure 12). The mannequin should be easily clothed utilizing off-the-shelf retail clothing sized appropriately for the stature of the mannequin.

5.7.1 Clothing Material

The most common material for clothing is cotton and polyester. According to Cotton Incorporated, 75% of men's clothing is made of cotton and 40% of women's clothing is made of cotton (http://www.cottoninc.com/fiber/quality/Fiber-Management/Fiber-Management-Update/05-Sept-2011/).

5.7.2 Clothing Color

According to the clothing color study of pedestrians as seen from the TASI one year naturalistic study of 110 cars, the most popular clothing colors are as shown in Figure 12 [18]. For easier selection of fabric for mannequin clothing, the acceptable ranges of the RGB values for the brightness variation to be a maximum of 10% (Table 4). For a balance of easy selection of clothing fabric and color, clothing color range is recommended to be within 10% brightness variation of the ideal color .

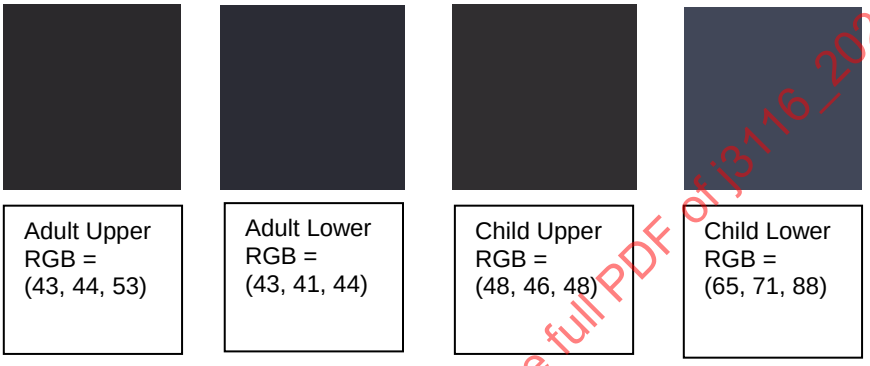

Figure 12 - The representation of upper/lower adult and upper/lower children clothing color from left to right

Table 4 - Comparison of clothing color ranges according the brightness variations

	Color	RGB values	Color Demonstration	Brightness variation range	Darker color	Lighter color	Acceptable range of RGB values
Adult lower clothing color	Black	43, 41, 44		±10%			43 ± 21, 41 ± 20, 44 ± 21
Adult upper clothing color	Deep dark blue	43, 44, 53		±10%			43 ± 21, 44 ± 21, 53 ± 23
Child upper clothing color	Black	48, 46, 48		±10%			48 ± 22, 46 ± 22, 48 ± 22
Child lower clothing color	Medium blue	65, 71, 88		±10%			65 ± 26, 71 ± 27, 88 ± 30

5.8 Infrared Reflection

The goal of specifying the IR reflectance of the pedestrian mannequin is for testing the performance of pedestrian detection by automotive Lidar. It should be clarified that infrared discussed here is near infrared and not far infrared used for body heat detection. Since the penetration depth of IR is in the level of micrometers, the IR reflectivity of pedestrians is contributed by their skin and clothing. Here the IR reflectance of skin and clothing of standard pedestrian mannequins are specified.

5.8.1 IR Reflectance of Pedestrian Mannequin Skin

Human skin reflectivity in various spectrums was measured in many decades [19, 20]. *In the 800 to 1100 nm wavelength range, the IR reflectivity of human skin is in the range between 0.4 and 0.6.*

5.8.2 IR Reflectance of Clothing Fabric

The IR reflectivity of clothing is a function of IR wavelength, the fabric material, fabric color, and fabric pattern. Cotton and polyester are the most common clothing material (especially for man and boy clothing). Based on the measurement of 98 samples of cotton and polyester fabric in a wide variety of color with a variety of patterns from two vendors who supply fabric to the clothing industry [21], *the recommended IR reflectance of the pedestrian mannequin clothing is 46 to 70% in the wavelength range of 800 to 1100 nm and 40 to 64% in the range of 750 to 800 nm. In addition, any fabric material can be used but shall be sufficiently thick such that it does not transmit any light through to the substrate of the mannequin that could result in a different apparent reflectance.*

5.9 Pedestrian Radar Cross Section

5.9.1 Background

Radar detects objects by transmitting radio signals towards a target and then recording the echoed radio signals reflected off the target. Common radar signal types include single-frequency continuous wave (CW) signal, multiple-frequency CW signal, amplitude-modulated (AM) CW signal, or frequency-modulated signal. The received power of the reflected signals from a target illuminated by the radar signal can be predicted via the well-known radar equation (see Equation 1).

$$P_r = \frac{P_t G_t}{4\pi r^2} \sigma \frac{1}{4\pi r^2} A_{eff} \quad \text{(Eq. 1)}$$

where:

P_t = power transmitted by the radar (watts)

G_t = gain of the radar transmit antenna (dimensionless)

r = distance from the radar to the target (meters)

σ = radar cross-section of the target (meters squared)

A_{eff} = effective area of the radar receiving antenna (meters squared)

P_r = power received back from the target by the radar (watts)

The term $\frac{P_t G_t}{4\pi r^2}$ represents the power density (watts/m^2) that the radar transmitter produces at the target. The total power (watts) intercepted and reflected by the target is the product of this incident power density and the target's radar cross-section (RCS), σ (m^2), i.e., $\frac{P_t G_t}{4\pi r^2}\sigma$ (watts). This reflected electromagnetic waves then produces a power density of $\frac{P_t G_t}{4\pi r^2}\sigma\frac{1}{4\pi r^2}$ at the radar receiver. The receiver antenna on the radar then collects this power density with its effective area, A_{eff} yielding the net received power predicted by Equation 1.

The "radar cross section (RCS)" is a normalized quantity that characterizes a target's ability to reflect radar signal with respect to the strength of the plane wave illuminating on the target and is defined as:

$$\sigma = \lim_{r\to\infty} 4\pi r^2 \frac{S_r}{S_i} = \lim_{r\to\infty} 4\pi r^2 \frac{|E_r|^2}{|E_i|^2} \quad \text{(Eq. 2)}$$

where S_i is the power density of the incident radar signals measured at the target, and S_r is the reflected power density seen at radar from a large distance r such that the magnitude and phase variations across the target area are nearly uniform; E_r and E_i, are the corresponding reflected and incident electric fields, respectively. Note that definition in Equation 1 requires plane waves as specified by the $r \to \infty$ condition which ensure uniform illumination over the entire target. In practice, such condition can be achieved at a shorter distance inside a Compact Range where a large parabolic reflector or dual reflectors can be used to produce collimated wave fronts, i.e., plane waves. If such a Compact Range is not available, the target distance r should satisfy

$$r > \frac{2D^2}{\lambda} \quad \text{(Eq. 3)}$$

where D is the maximum cross sectional dimension of target under test, and λ is the operating wavelength. It should also be pointed out that Equation 1 assumes frequency-domain data and is applied at each frequency separately since RCS of a target usually varies with frequency.

Since RCS is normalized against the radar signals arriving at the target, it is a property of the target alone independent of the radar, antennas, and waveforms. Therefore, RCS allows for comparing the radar reflectivity of different targets and the performance of different radar systems against the same reference target. This makes RCS an ideal parameter to quantitatively compare the reflectivity of a radar mannequin with the reflectivity of real pedestrians.

However, the far-field condition in Equation 2 may not be applicable to millimeter-wave radars used for automatic emergency braking (AEB) applications where the target distance of concern is usually less than 100 m. For instance, Equation 2 requires a minimum distance of 46 m at 77 GHz for target size of 30 cm. The non-uniform phase illumination across a target closer than Equation 2 condition results in weaker radar response [22] compared to the far-field RCS value in Equation 1. A recommended calibration procedure for obtained RCS at any target distance can be found in Appendix B. This RCS decreasing trend as the pedestrian distance decreases has been reported in the EU FP7 ASSESS project report [23]. Other factors which can affect the response of pedestrians perceived by radar include pedestrian body shape, motion, posture, viewing angle [24] and vertical beam pattern of antennas, etc.

Therefore, in order to accurately assess the effectiveness of AEB radars in detecting pedestrians using surrogate radar mannequins, the surrogate needs to be able to produce similar radar responses as real pedestrians under test scenarios specified by relevant standard AEB test protocols [25]. This should be done by demonstrating that the RCS of the surrogate meets the RCS requirements established based on the measured or validated simulation RCS data of real pedestrians under scenarios specified by relevant standard AEB test protocols.

5.9.2 Pedestrian RCS Features at 76 to 78 GHz

The radar response from a pedestrian is affected by the following factors:

- illumination region
- body shape and size
- angle of incidence (or look angle)
- posture of the pedestrian
- distance to radar
- clothing on the pedestrian
- articulation of arms and legs

Effect of Illumination Region

The radar beam widths of 76 to 78 GHz radar can be very small and may not fully illuminate the entire body of the mannequin. In this case, the magnitude and pattern of the radar response depend on where the radar illumination region is. Figure A2 in Appendix A compares the RCS patterns of head, arms, legs, and torso of an adult with numerical model simulations. These results show that the torso produces highest RCS level due to its larger flat area. If the radar beam illuminates multiple parts of the pedestrian, the resultant radar response is the summation of complex (magnitude and phase) scattered fields from different regions on the body.

Effect of Body Shape, Size, and Posture

The radar response of pedestrians is related to the “cross section” of the body as well as destructive and constructive interference of scattered fields from different parts of body due to their different local shapes, sizes [26], and distances to the radar. Therefore, the radar response depends on body shape, size, and posture. For instance, an obese person has different local body curvature and cross section area, which produce quite different RCS pattern compared to a fit person (Figures A3 and A4). Also, adult and child will produce different RCS magnitude and patterns (Figures A5 and A6). The measured smoothed RCS pattern of a 7-year-old child varies between -20 and -10 dBsm, which is about 6~8 dB lower than that of a young male adult. Also the RCS pattern of child shows less variation at different view angle and a generally circular shape.

The same person can also produce a very different radar response in different postures such as standing, walking, and running, as a result of different relative angles and distances of the body parts, as demonstrated in Figures A9 to A13.

Effect of Angle of Incidence (or Look Angle)

Due to the very short wavelength (~3.9 mm at 77 GHz) as well as the high dielectric constant (6~8) and conductivity (38 to 42 S/m) of human skin tissue, the radar response are dominated by reflections from the surface where it is directly illuminated by the radar beam [27]. Multiple bounces on the body and shadowed body part play little role in contributing to the mm-wave radar response. Since the horizontal cross section of human body is not uniform, and defined mainly by the contour of the torso and positions of the arms and legs in different postures, the radar response of pedestrian will vary significantly with horizontal look angle. In fact, the raw, unsmoothed radar response of an average adult could change from a local maximum to a local minimum in 0.4 degrees as seen in many simulated and measured RCS patterns shown in Appendix A. Figure 13 shows the numerical model simulated 77 GHz RCS patterns and distributions around 360° of azimuth angles for a 1.8 m tall male adult and a 1.26 m tall child. It shows that most RCS level concentration occurs around -3 dBsm for the standing adult, and a similar -6 dBsm for the running adult and standing child.

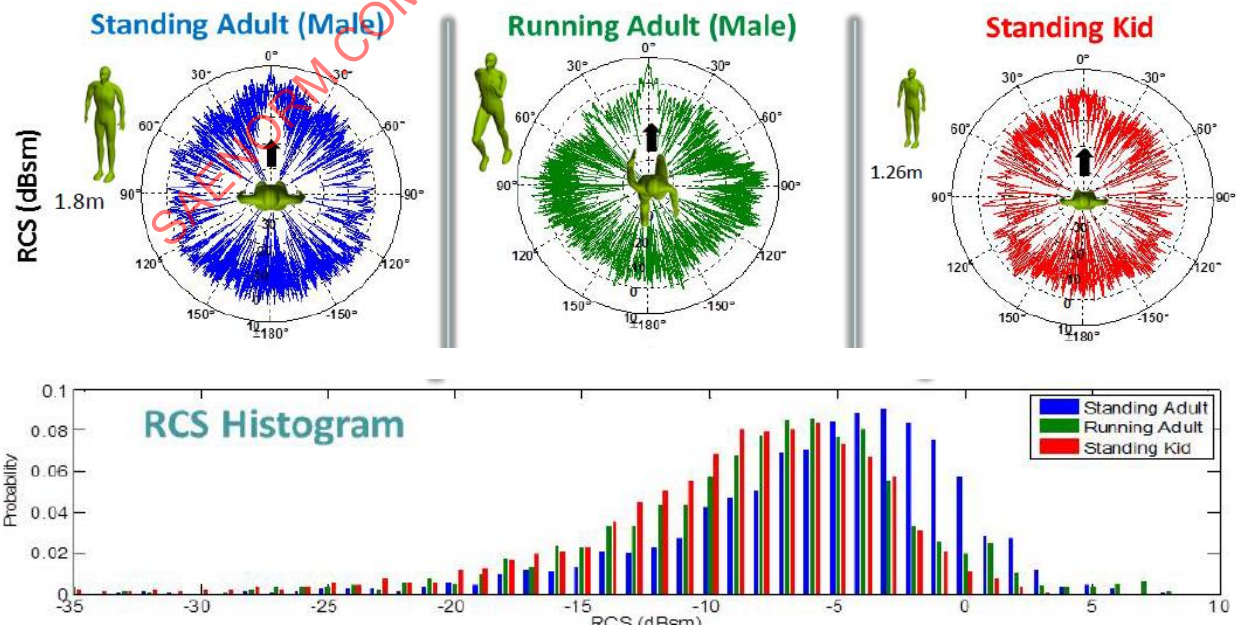

Figure 13 - The numerical model simulated 77 GHz RCS patterns and distributions around 360° of azimuth angles

The rapid magnitude oscillation in the raw RCS pattern suggests that detection based on unprocessed real-time instant received power of the radar response would not be practical. To alleviate this rapid variation issue, angular smoothing, time-averaging, or frequency average can be used. For instance, 5° moving averaged RCS patterns (Figures A9 to A13), allows one to better understand the global RCS variation as a function of horizontal look angle. Stronger radar response of pedestrian usually occurs near the front and rear look angles where the physical cross section viewed from radar is maximal as shown in Figure A14 which shows that the mean RCS value a group of 9 human subjects (Figure A8 and Table A1) exhibits an elliptical shape of pattern with RCS value ranging approximately from -10 to -5 dBsm, which corresponds to the RCS obtained from a shorter range (~10 m). The effect of distance to radar on RCS will be discussed in the next section.

Effect of Distance to Radar

Traditional radar applications deal with targets located in the far field as defined in Equation 2, which corresponds to approximately 82 m at 77 GHz for a body width of 40 cm if we assume torso to be the dominant scattering mechanism. This condition ensures the phase of electromagnetic waves illuminating upon the entire width of the pedestrian under test is relatively uniform, i.e., less than 45°. Under this far-field coherent phase condition, targets usually produce maximum reflectivity as a result of constructive interference from reflections from different regions on the target. For instance, the RCS values listed Table B1 assume plane waves of incidence. Since most collision avoidance systems and automatic emergency braking systems (AEB) are designed for detecting pedestrians operate at distances closer than the Equation 2 condition, this means that the magnitude and phase of the radar signals illuminating over the width of the pedestrian would vary significantly. It results in reduction of the net reflected power because of non-coherent interference of reflected signals from different parts of the body. This phenomenon has been studied and reported by Falconer (1988)[28] with the figure shown in Figure A26.

In addition to the above non-coherent scattering condition, short target distance could also lead to partial illumination of the radar signal on the pedestrian target due to the narrow antenna beam width of most 76 to 78 GHz radars. This partial illumination effect can also lead to change in RCS since different body regions produce different scattering magnitude and patterns as discussed previously. This RCS value reduction, however, should not be confused with the fact that actual received reflected power from the pedestrian will increases as distance decreases due to less $1/R^4$ propagation loss. The decreasing rate of target RCS as distance decreases strongly depends on the radar beam width and height. For instance, a narrow beam radar mounted at the same height as torso will likely exhibit slower decreasing rate at short distance (<10 m) compared to a radar mounted at the height below the waist.

The aforementioned decreasing target RCS phenomenon at short distance was observed and documented in ISO/WD 19206-2 and is replotted in Figure A28. Notice that the trend is very similar to the trend predicted in Figure A27 based on the phase incoherency effect for distance greater than 8 m. Figure A29 shows another measurement example of front-view RCS of a stationary standing male human subject (height of 185 cm and weight of 76 kg) at 77 GHz from 2 to 10 m in 30 cm increments. The data were calibrated against a trihedral corner reflector with 10 dBsm RCS. The reflector was placed at the same height (50 cm) as the radar and at several different distances from 7 to 11 m in 30 cm increments. This calibrated RCS result as function of target distance agrees well with Figure A28. The oscillatory behavior as a function of target distance is caused by multipath effects of ground surface reflections.

Effect of Clothing

In most cases, dry clothing made of light thin fabric has no effect on radar response of pedestrians in the 76 to 78 GHz frequency range. This is demonstrated in Figure A18 where the moving-window standard deviation of RCS patterns and smoothed RCS patterns of a male subject dressed in shorts and T-shirt are compared with simulation results of the undressed results obtained from a numerical model of the human subject. Figure A19 shows pictures of a male subject dressed in different seasonal clothing. The corresponding measured RCS STD patterns and 5° smoothed RCS patterns are compared in Figure A20. The RCS pattern data were collected from -10 to 190° in 0.2° steps. From these results, it is observed that:

- thicker clothing effectively increases the body's side-to-side width, thus raising RCS level in the front and back directions, and
- thicker clothing also increases the rotational symmetry, i.e., reducing the detail cross section contour variation, reducing RCS deviation.

Therefore, the clothing effect on pedestrian RCS is not significant except for special clothing materials or conditions, such as clothes made of leather, clothes with excessive metal parts, or wet clothes.

Effect of Arm and Leg Articulations

Real-world pedestrians on the street will likely be either walking or running with moving arms and legs. Figure A21 shows high-speed camera captured velocity profiles of different body parts of a human subject during fast walking and slow running. It shows that points on legs and arms have different periodic acceleration and deceleration gait cycles, which is approximately 1.45 Hz for walking gait and 3.1 Hz for running gait. Since legs and arms produce significant radar response as discussed previously, it is expected that the articulations of legs and arms during walking or running will produce additional frequency shifts (i.e., micro-Doppler effect) on top of the frequency shift (Doppler effect) associated with the pedestrian's walking or running speed relative to the radar. The corresponding simulated spectrum of 77 GHz radar response are also shown at the bottom of Figure A21. Note that these responses were calculated by modeling a human as a composition of multiple connected perfectly conducting ellipsoids (see Figure A22) and using a closed-form RCS formula for a perfectly conducting ellipsoid [29]. It is observed that moving legs and arms produces periodic micro-Doppler frequency modulations on top of the main Doppler frequency (middle slow-varying spectral line) which is associated with the torso velocity. The micro-Doppler effect is stronger in the along the road motion scenarios than the crossing road scenarios. The maximum Doppler frequency shifts are around 720 Hz and 1400 Hz for the fast walking case and running case, respectively, which corresponds to a walking speed of 1.42 m/s and running speed of 2.76 m/s, respectively.

The amount of micro-Doppler components contained in radar responses depends on the instantaneous receiver bandwidth and the amount of illumination on the arms and legs, especially the legs. More specifically, the receiver needs to have at least 2 kHz instantaneous bandwidth in order to be able to observe the micro-Doppler features of a running pedestrian. In addition, more illumination on the legs produces stronger micro-Doppler responses associated with legs as demonstrated in the measured responses (Figures A23 and A24) obtained from radar heights of 50 cm, 75 cm, and 100 cm.

5.9.3 RCS Requirements of Pedestrian Mannequin in 76 to 78 GHz

The 76 to 78 GHz RCS properties of pedestrians obtained from both theoretical and experimental data were discussed in the previous sections. Based on these data, a minimum set of RCS performance requirements should be met by any pedestrian mannequin intended for evaluating the effectiveness of 76 to 78 GHz radars in detecting pedestrians so that the mannequin produces similar radar responses as real pedestrians. These requirements are discussed below.

1. RCS Level and Pattern Requirements

The RCS requirements below are referred to the local (i.e., within a small horizontal angle region) average RCS value of the mannequin without multipath effect. These values are specified when the mannequin is in standing position with both arms and legs in the vertical positions. Note that the RCS value for distance closer than 10 m will decreases as distance decreases. However, the decreasing rate depends on the radar height and antenna beam shape, and thus is unspecified.

Adult

The RCS level of an adult mannequin as a function of azimuth angle should have an elliptical pattern with maximum axis being along the front-to-rear direction and minor axis being along the side-to-side direction.

Far-Field

Front/Rear RCS: 0 dBsm ± 5dB
Side RCS: -5 dBsm ± 5dB
360 mean RCS: -3 dBsm ± 5dB

At 30 m

Front/Rear RCS: -1 dBsm ± 5 dB
Side RCS: -6 dBsm ± 5 dB
360 mean RCS: -4 dBsm ± 5 dB

At 20 m

Front/Rear RCS: -3 dBsm ± 5 dB
Side RCS: -8 dBsm ± 5 dB
360 mean RCS: -6 dBsm ± 5 dB

At 10 m

Front/Rear RCS: -5 dBsm ± 5 dB
Side RCS: -10 dBsm ± 5 dB
360 mean RCS: -8 dBsm ± 5 dB

Child (Circular RCS Pattern)

The RCS level of a child mannequin as a function of azimuth angle should have a circular pattern.

>10 m

360 mean RCS: -10 dBsm ± 5 dB

2. Micro-Doppler Effect

To evaluate the performance of radars that utilize micro-Doppler as detection features, the arms and legs of the pedestrian mannequin for this purpose should have similar articulations and gait cycles as real walking or running pedestrians. Leg articulations are more important than arms. However, articulated legs and arms do not guarantee the production of correct micro-Doppler features in measured radar response. The legs and arms also need to be able to have proper RCS levels and patterns as demonstrated by the numerical model simulated results shown in Figure A1. These results show that the RCS of the legs and arms have approximately uniform azimuth patterns and have average RCS levels of approximately -15 and -18 dBsm, respectively. For radar detection purpose, it is possible to just require the legs to be articulated as long as they have proper RCS levels and gait cycle.

5.10 Safety Considerations

The mannequins should be light weight (recommended limit: adult not to exceed 7 kg and child not to exceed 4 kg) and should not include hard surfaces or sharp points such that they do not expose the test vehicle occupant to significant risk of personal injury. It is recommended that the mannequins be designed such that they are not likely to cause substantial (other than cosmetic) test vehicle damage when impacts occur during tests up to 60 km/h relative speeds. In the event that a mannequin is struck by the test vehicle, the mannequin should be able to proceed in a trajectory over the top of the vehicle or to the side of the vehicle. The mannequin and any associated support structures should not be designed such that the mannequin will be easily pulled under the wheels of the moving test vehicle during normal test conditions.

If the test vehicle is not protected, some minor damage to the vehicle body might be experienced during higher speed impacts. To reduce the risk of vehicle damage, protective devices (fabric or film coverings, auxiliary structures, auxiliary padded bumpers, etc.) may be add to the test vehicle. However, great care must be exercised to insure that these devices do not impede the function of the sensing systems to properly detect the pedestrian target. The best method is to design, manufacture, and install all protective devices such that they do not enter the field of view of any sensing system or otherwise cause distortions of the sensing system responses.

Due care should be exercised when deciding whether any exterior pedestrian protection devices or interior occupant protection devices (deployable hoods, airbags, seatbelt pretensioners, etc.) should be disabled during pedestrian PCS testing.

Due care should be exercised when deciding whether the test vehicle occupants should wear protective face or eye protection (in case impact with the mannequin causes windshield damage).

5.11 Vertical Support

The pedestrian target should be able to be maintained and stabilized in the desired upright position in order to best represent a real human pedestrian. If necessary, this may be accomplished via devices (rods, tubes, cables, strings, cords, etc.) extending from any structures used to support or convey the target either from above or from below. When these devices are utilized, great care should be exercised to insure that these devices do not impede the function of the sensing systems to properly detect the pedestrian target, and do not present a substantial chance of hazard to the occupants and/or damage to the car.

5.12 Durability and Maintainability

In order to minimize test cost and time requirements, the mannequin should be resistant to permanent damage during impact with the test vehicle. If the mannequin is designed such that portions of the mannequin can separate during an impact with the vehicle, the mannequin should be able to be reassembled within 5 minutes (this does not include the setup time of the stabilization/conveyance system). If permanent mannequin damage is caused by an impact, the pedestrian mannequin should be repairable at the test site utilizing replacement components (if necessary) and simple hand tools. When these types of repairs are made, great care should be exercised to insure that the repairs do not impede the function of the sensing systems to properly detect the pedestrian target.

5.13 Environmental Conditions

The pedestrian mannequin should be usable and functional under normal test facility environmental conditions as follows:

- Temperatures from -5 to 40 °C
- Mannequin should function properly and smoothly when wind conditions do not exceed 6.7 m/s (15 mph) peak speeds during gusting conditions
- Mannequin is not expected to be utilized during inclement weather. However incidental exposure to rain or other moisture should not have a lasting detrimental effects on the sensor responses (e.g., RCS values for radar sensors)
- The mannequins shall not deform or otherwise be damaged when stored under temperatures between -40 and +80 °C.

6. NOTES

6.1 Revision Indicator

A change bar (I) located in the left margin is for the convenience of the user in locating areas where technical revisions, not editorial changes, have been made to the previous issue of this document. An (R) symbol to the left of the document title indicates a complete revision of the document, including technical revisions. Change bars and (R) are not used in original publications, nor in documents that contain editorial changes only.

PREPARED BY THE SAE ACTIVE SAFETY SYSTEMS STANDARDS COMMITTEE OF
THE DRIVER ASSISTANCE SYSTEMS STEERING COMMITTEE

APPENDIX A - RCS OF PEDESTRIAN IN 77 TO 78 GHz

A.1 RADAR SCATTERING MECHANISMS OF PEDESTRIAN

At 76 to 78 GHz, the human body is a relatively large scatter in terms of wavelengths. The high permittivity and high conductivity of human skin also means that little radar signals can penetrate deep into skin [30]. Therefore, most radar scattering in this frequency range is produced via reflection at the skin surface. As a start, it would be insightful to compare the RCS from different part of human body so that one can focus on dominant scattering mechanism when preparing for a radar mannequin. Obviously, this would be difficult to do via experiments. Therefore, numerical model simulations were used to calculate the RCS contributions from four major body parts: head, torso, arm, and legs as shown in Figure A1. All models were made of homogeneous material with the electrical property of dry human skin [31].

Figure A2 plots the simulated RCS patterns of the head, torso, arm, and legs at 77 GHz. These results showed that the torso dominated the scattering for most look angles, with a maximum of approximately 1 dBsm occurring near the rear look angles (±170°). The next strongest scattering came from the legs, which produced approximately -1 dBsm, occurring at certain narrow look-angle regions (±0°, ±30°, ± 120°), likely related to the corner-reflector effect from the two legs.

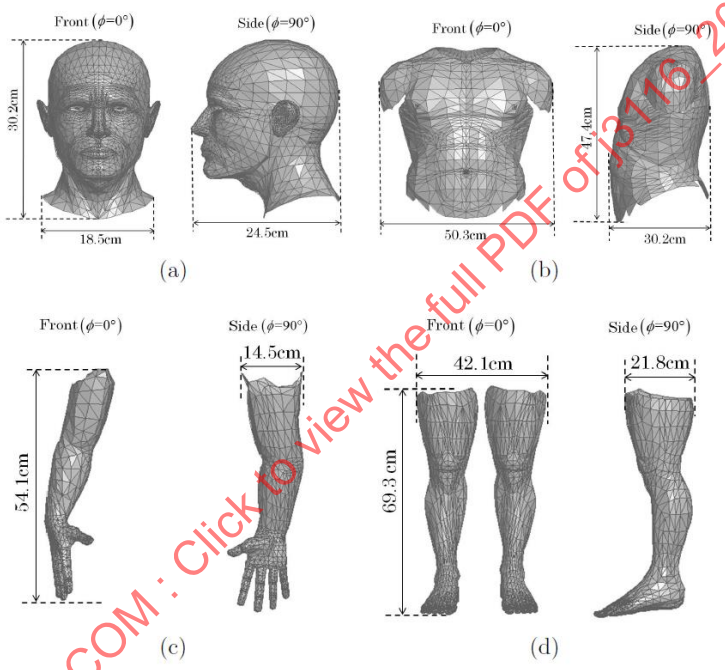

Figure A1 - The numerical models of the four major human body parts: (a) head (b) torso, (c) arm, and (d) legs

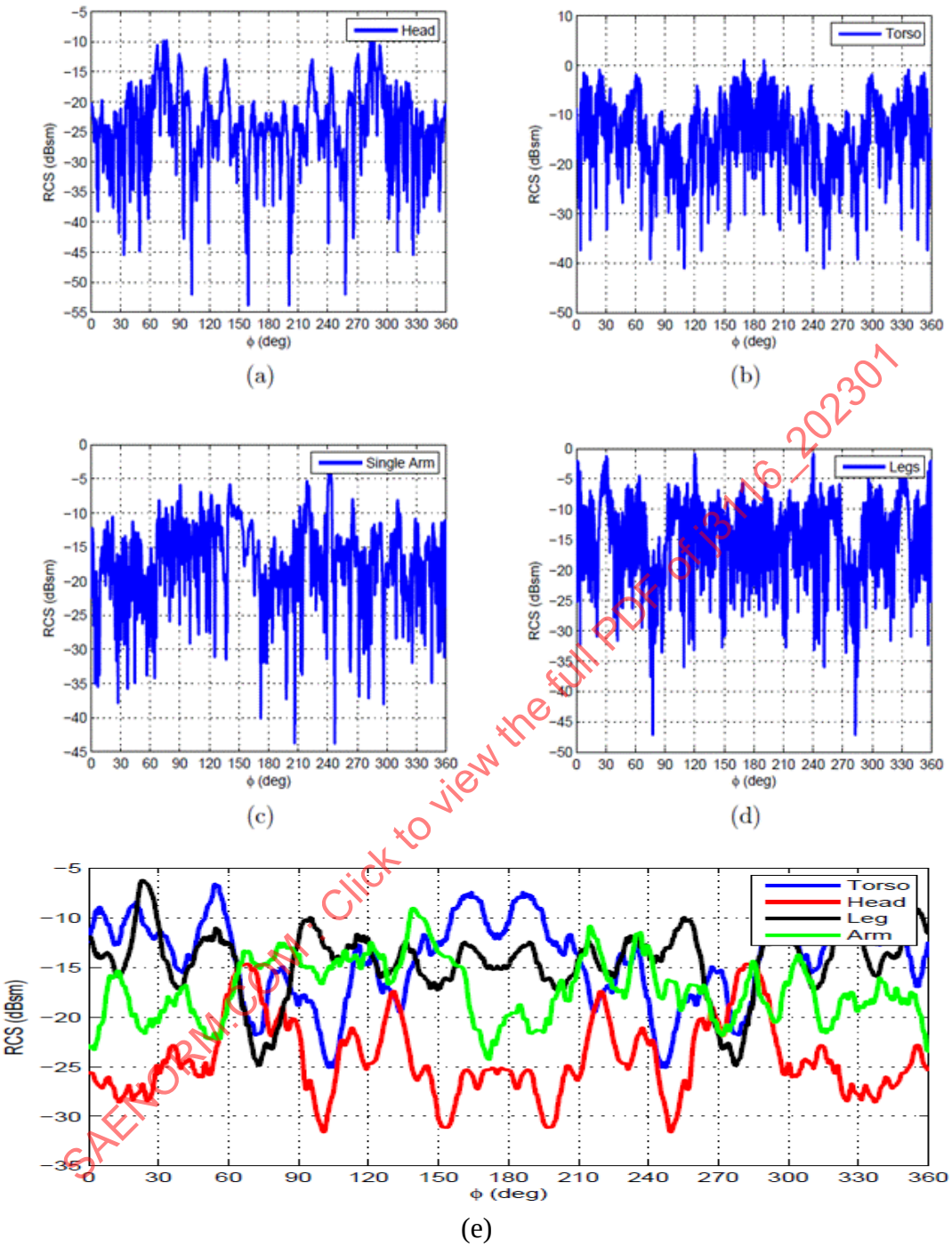

Figure A2 - The simulated 77 GHz RCS patterns of the four major human-body parts shown in Figure A1: (a) head, (b) torso, (c) arm, and (d) legs and (e) comparison of 5° smoothed azimuthal RCS patterns

A.2 EFFECT OF BODY SIZE ON PEDESTRIAN RCS

The simulated RCS pattern of a physically fit person and obese person are compared in Figure A3. Obese person normally has a much larger torso thickness compared to physically fit person, especially at the waist and belly part. As is seen in Figure A3, different from the physically fit person, the peak RCS of the obese person appears at around 30 to 60°, where the body thickness can be seen by the radar wave. Such feature was verified by measured RCS pattern of fit and obese person as shown in Figure A4.

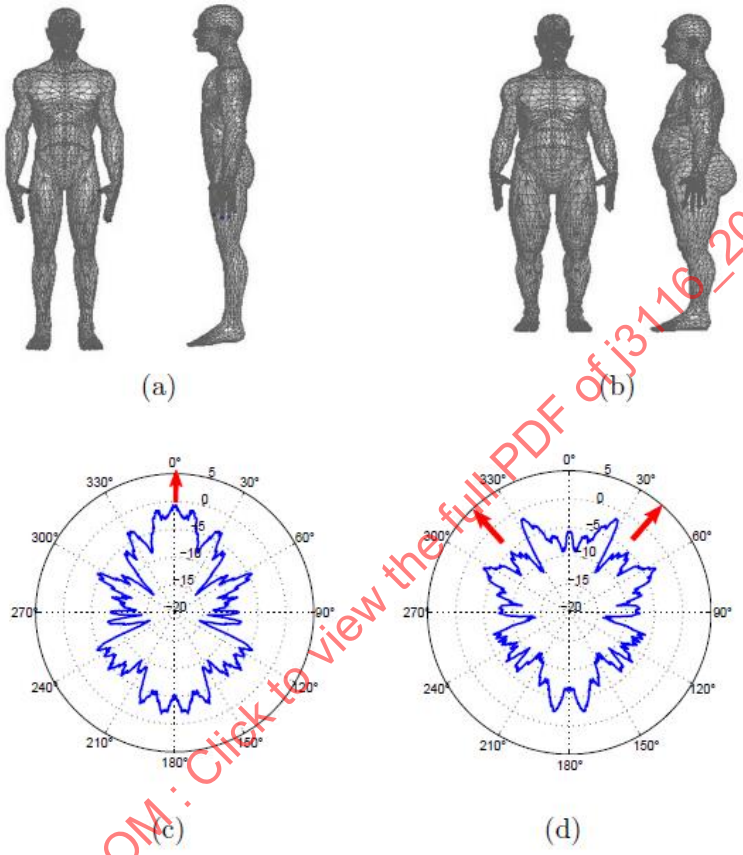

Figure A3 - Comparison of simulated 5° smoothed RCS patterns at 77 GHz between physically fit and obese subjects

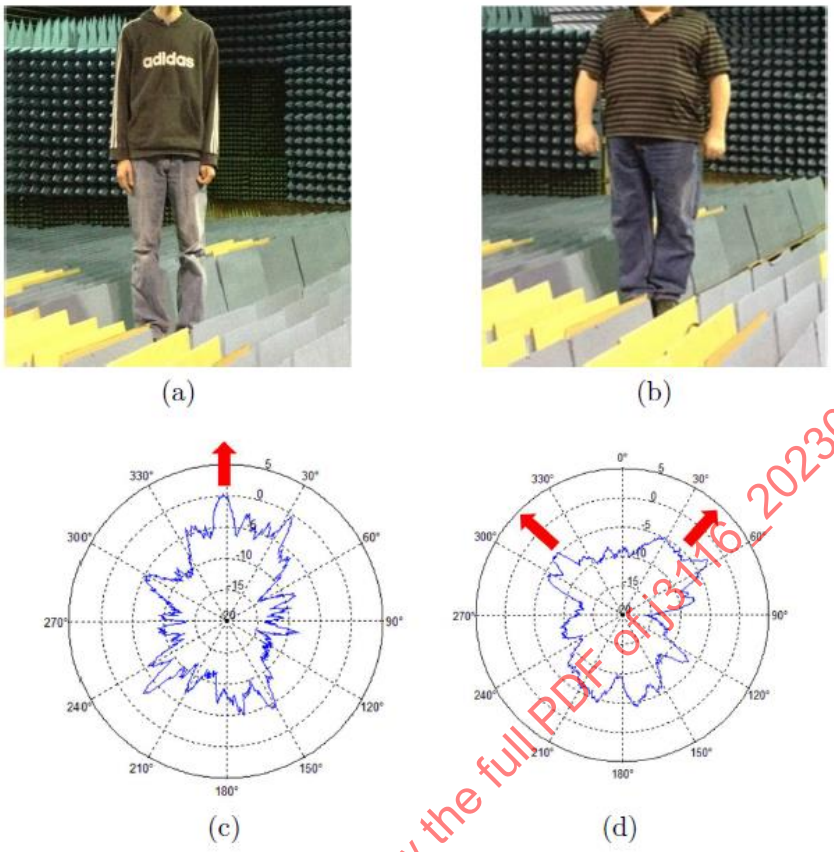

Figure A4 - Comparison of measured 5° smoothed RCS patterns at 77 GHz between physically fit and obese subjects

The simulated RCS pattern of adult male and child are compared in Figure A5. The height of adult male and child are 1.8 m and 1.26 m, respectively. The dimension of the child model is obtained from measured physical dimension of the child subject. Due to smaller cross area, child's RCS level is about 5 to 8 dB lower than adult. Child's torso thickness has smaller differences between front-to-back direction and side-to-side direction. Therefore, RCS pattern of child is closer to circular shape compared to the elliptical shape of RCS pattern of adult.

The measured RCS pattern of a 7-year old child is presented in Figure A6. The 5° smoothed RCS pattern of child varies between -20 and -10 dBsm, which is about 6~8 dB lower than the RCS level of adult. Also, the RCS pattern of child shows less variation at different view angle and a generally circular shape.

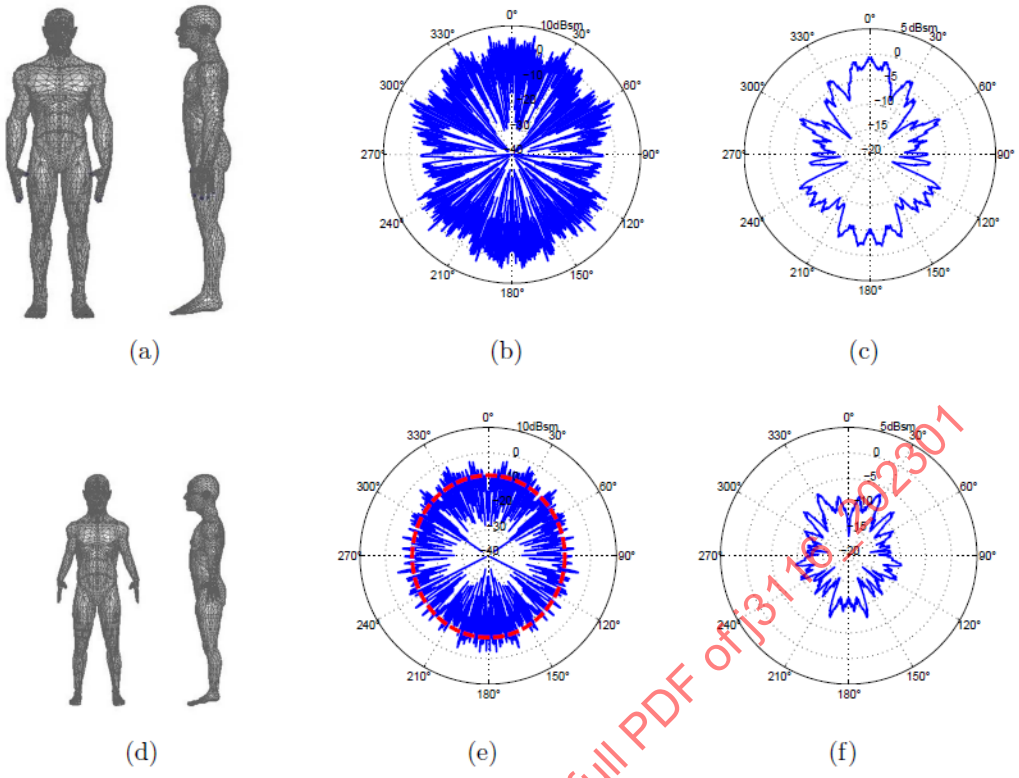

Figure A5 - Comparison of simulated RCS patterns of adult male and child subjects

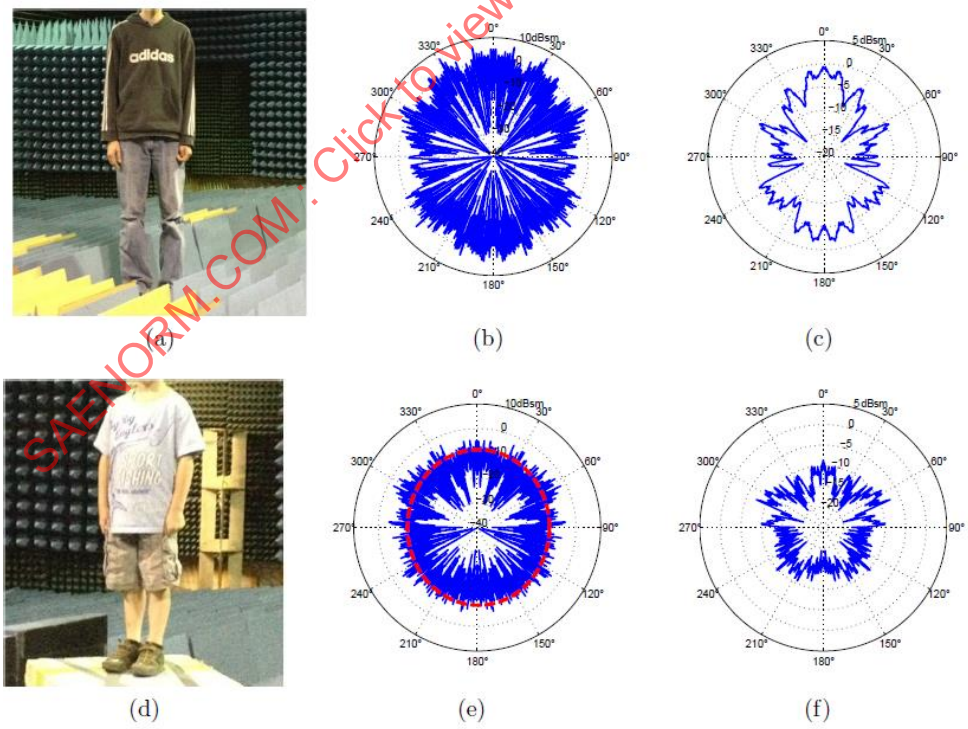

Figure A6 - Comparison of measured RCS patterns of adult male and child subjects

A.3 EFFECT OF VIEW ANGLE ON PEDESTRIAN RCS

In time domain, the scattering off a uniformly illuminated human is dominated by the upper body. This is demonstrated by the simulated impulse response pattern of an adult male as shown in Figure A7. The impulse contains uniform spectrum from 76 to 78 GHz. The body is made of uniform dry skin tissue. The arrival time of the peak response at different azimuth view angle traces out a contour (right figure) that is very close to the physical contour of the human's upper body.

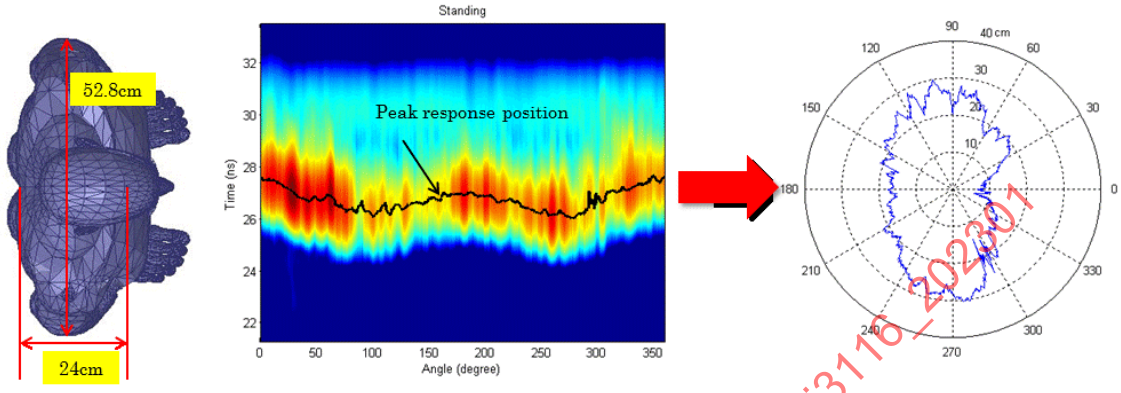

Figure A7 - Simulated 76 to 78 GHz impulse response of an uniformly illuminated male as a function of view angle

In frequency domain, the measured RCS level of a pedestrian varies significantly with view angle in the 76 to 82 GHz frequency range due to large body width in terms of wavelengths. To demonstrate this, the 77 GHz RCS patterns of nine human subjects (Figure A8) were collected inside an anechoic chamber. The front view angle corresponds to 0°. The physical dimensions of these human subjects are listed in Table A1. The RCS patterns at 77 GHz for five human subjects in standing and walking postures are shown from Figures A9 to A13 where the left plots are calibrated RCS patterns in 0.2° increments, the middle plot is the standard deviation of RCS values in dB evaluated with a 5° running window, and the right plot is smoothed pattern using a 5° moving average window. The smoothing helps visualizing global pattern features without the rapid fluctuations caused by in-phase and out-of-phase scattering interferences from different body parts that arrive at the radar at different time. The data were collected with the subject in stationary standing (top row) and walking posture (bottom row).

Figure A14 compares the average of smoothed RCS patterns at 77 GHz of all nine human subjects with the smoothed RCS pattern of a TASI mannequin [32] in standing posture. This results shows that the average RCS pattern from the nine human subjects exhibits an elliptical shape with its major axis lying along the front-to-back direction with RCS level of around -6 dBsm. The minor axis of the ellipse lies along the side-to-side direction with a RCS level of around -11 dBsm. Figure A14 shows that the TASI mannequin produces a RCS level and pattern similar to that of an average human in standing posture.

Figure A8 - Pictures of human subjects used in RCS measurements

Table A1 - Physical dimensions of human subjects for 76 to 77 GHz RCS data collection

Subjects	#1	#2	#3	#4	#5	#6	#7	#8	#9	Mean
Height	185.42	172.72	162.56	187.96	180.34	157.48	154.94	165.1	180.34	168.40
Weight (lb)	195.5	120.5	142.5	162.5	218.5	124.0	119.0	165.5	280.0	169.8
Head circum.	62.48	55.37	56.13	57.912	58.42	57.15	53.34	53.34	60.96	56.64
Head height	23.62	21.84	19.05	19.812	21.59	22.86	15.24	19.05	21.59	20.57
Neck circum.	38.1	36.7	35.3	34.80	40.64	33.02	33.02	40.64	50.80	38.1
Neck length	8.89	6.35	5.08	5.08	5.08	6.35	3.81	6.35	5.08	5.84
Shoulder width	46.74	40.64	41.91	47.24	45.72	38.1	36.322	45.72	50.8	43.43
Chest width	39.88	31.75	38.1	38.608	35.56	30.48	28.702	34.29	43.18	35.31
Waist circum.	93.98	71.12	92.71	80.01	99.06	78.74	81.28	96.52	132.08	91.44
Hip circum.	101.6	76.2	99.06	86.36	109.22	96.52	85.852	104.14	137.16	99.31
Torso length	43.18	38.1	38.61	38.1	39.37	33.02	35.56	36.83	40.13	37.59
Upper-arm circum.	31.75	23.11	33.02	30.48	29.21	26.67	25.4	30.99	38.10	29.97
Upper-arm length	24.13	27.94	21.59	24.13	22.61	29.21	31.75	27.43	30.48	27.68
Lower-arm circum.	27.94	20.32	22.86	20.07	22.86	19.05	22.86	27.43	32.51	24.13
Lower-arm length	32.00	25.4	19.05	27.94	26.67	25.40	24.13	26.67	27.94	2A1
Upper-leg circum.	53.85	46.74	50.8	54.61	63.5	48.26	45.72	68.58	63.50	54.36
Upper-leg length	35.56	36.83	35.05	41.91	39.37	48.26	38.10	34.29	35.56	38.1
Lower-leg circum.	36.32	31.50	33.78	41.91	43.18	36.83	33.02	40.64	48.26	38.1
Lower-leg length	44.70	40.13	35.56	40.64	39.10	36.83	38.50	35.56	45.72	39.12

NOTE: Unit in cm (unless specified otherwise).

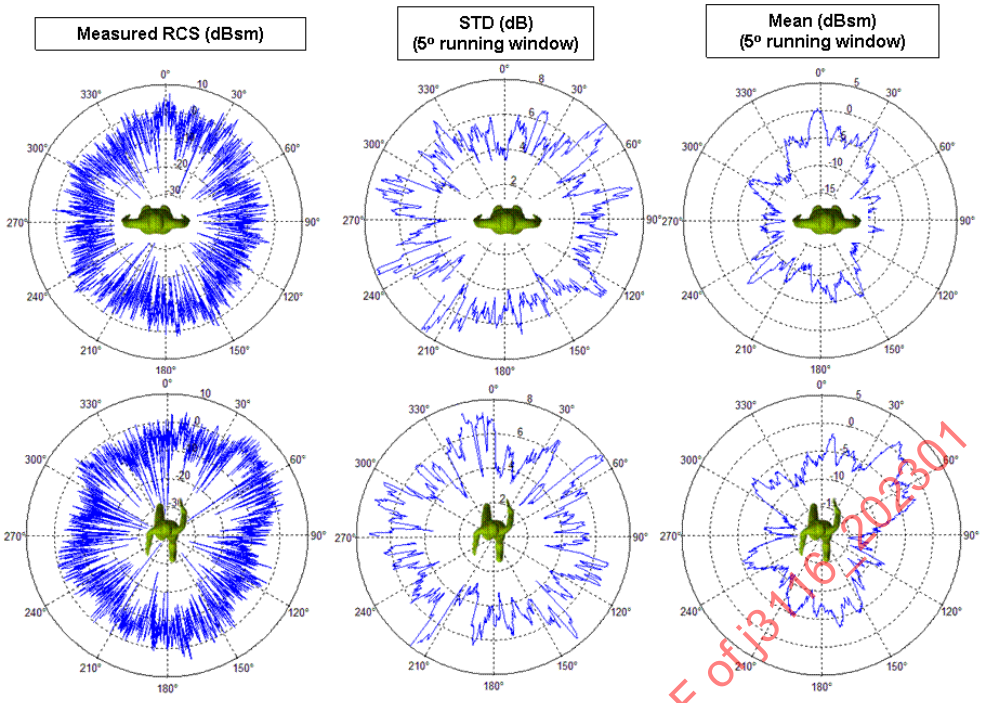

Figure A9 - Measured RCS data for subject #1 - (top) standing posture (bottom) walking posture

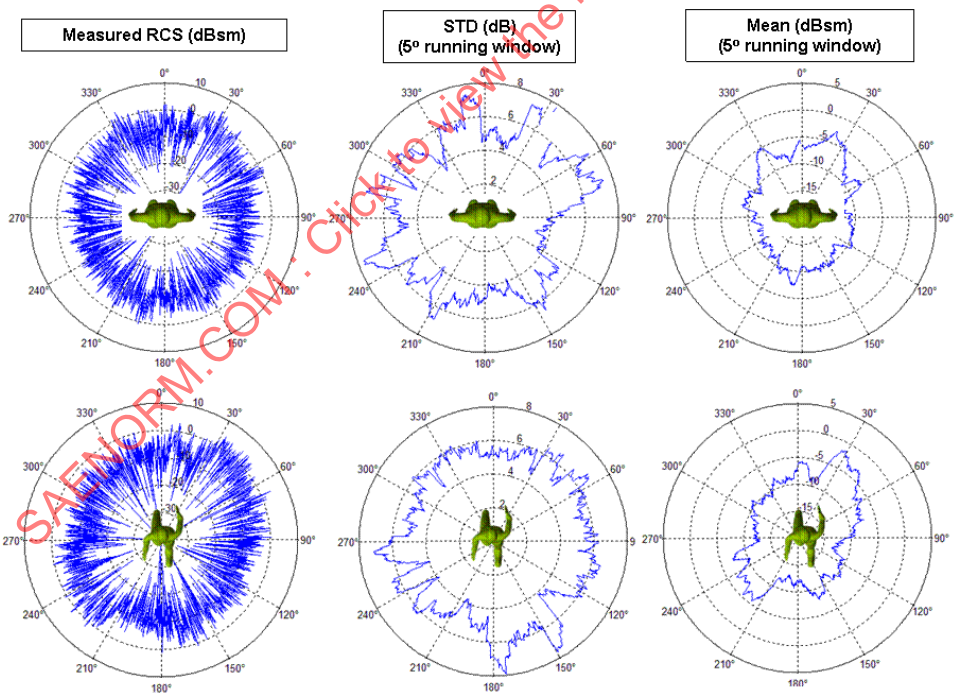

Figure A10 - Measured RCS data for subject #2 - (top) standing posture (bottom) walking posture

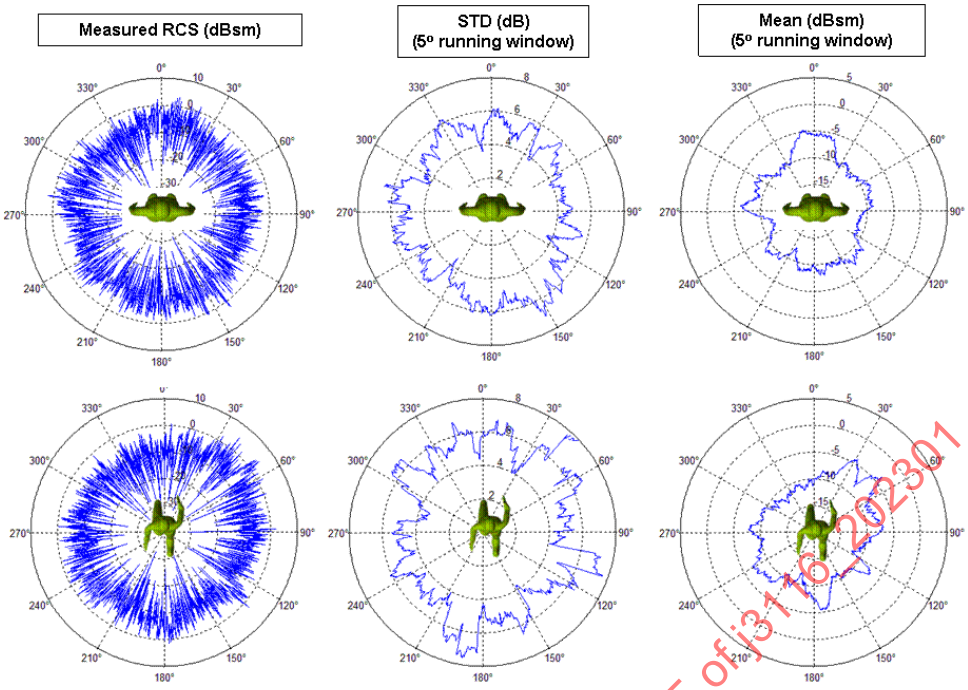

Figure A11 - Measured RCS data for subject #3 - (top) standing posture (bottom) walking posture

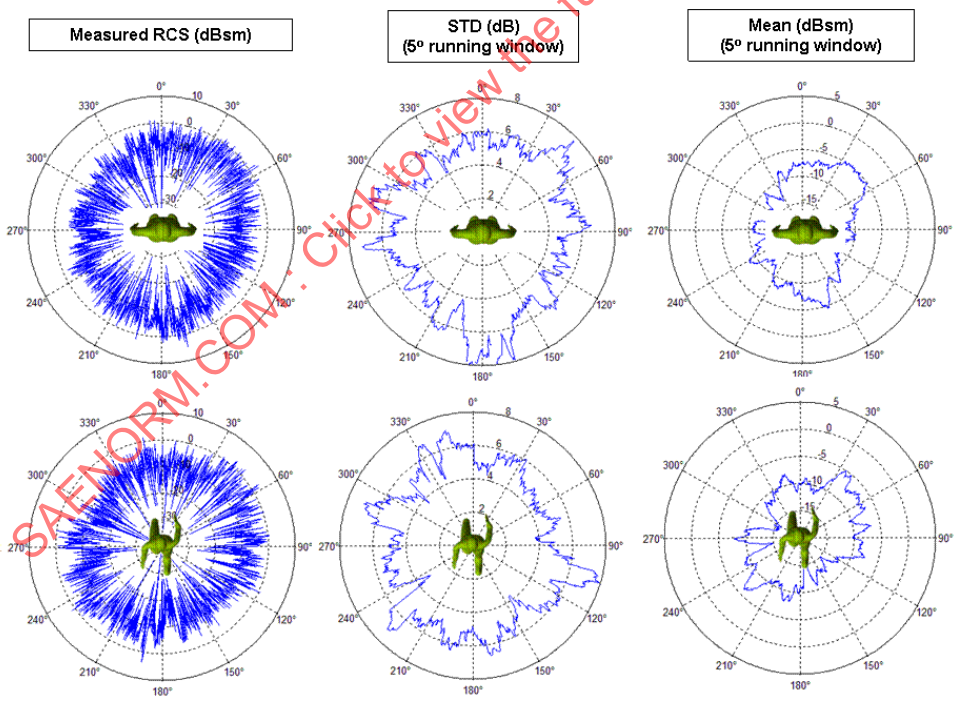

Figure A12 - Measured RCS data for subject #4 - (top) standing posture (bottom) walking posture

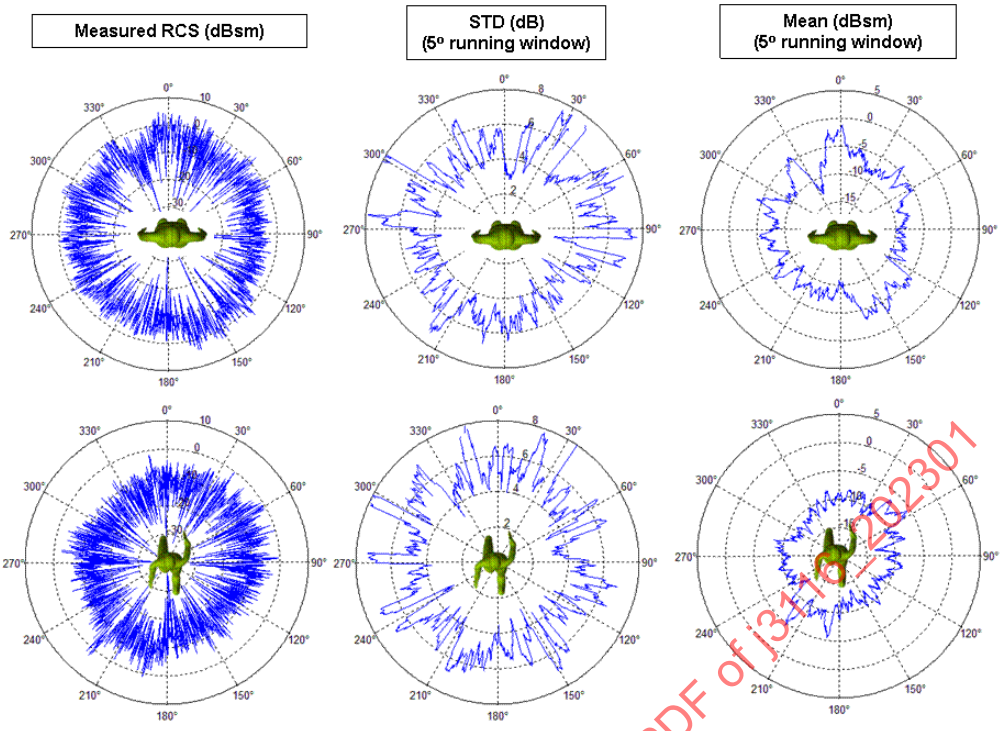

Figure A13 - Measured RCS data for subject #5 - (top) standing posture (bottom) walking posture

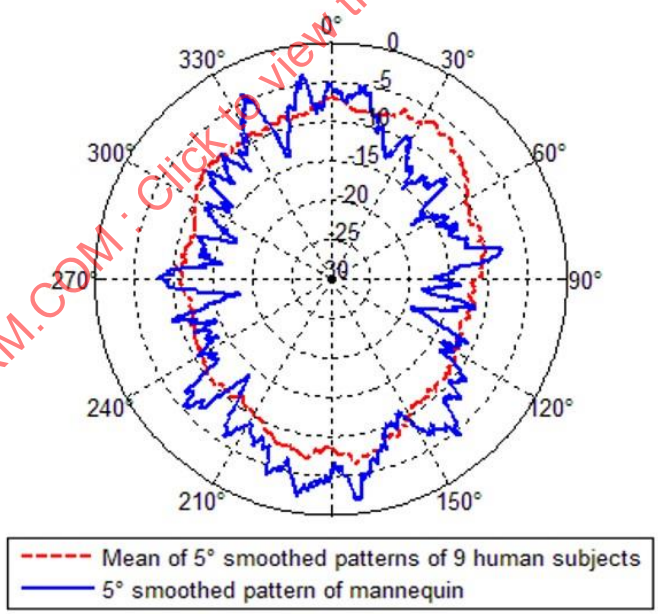

Figure A14 - Comparison between measured 5° smoothed RCS pattern of TASI mannequin and the average of the 5° smoothed RCS pattern of 9 human subjects in standing posture shown in Figure A8

A.4 POSTURE EFFECT ON PEDESTRIAN RCS

Comparing the smoothed RCS patterns between standing and walking postures from Figures A9 to A13 shows similar maximum RCS level. However, the maximum RCS in the walking posture case does not occur in the front and back directions as in the standing case. Figure A15 summarized the smoothed RCS patterns of human subjects 1 to 4 in walking postures. The measured results show that the maximum RCS directions occur at approximately 30 to 45° from the front, consistent with the rotation of upper torso. To further investigate this observation, two numerical model simulations were conducted for the walking posture as shown in Figure A16. One simulation contains offset arms without rotating upper torso. The other simulation has the same offset arm positions but also has a rotated upper torso. It shows that maximum smoothed RCS pattern only rotates in the case where upper torso is rotated. This finding is important in that if the mannequin is to produce similar pattern changing effect, its upper torso will have to mimic the rotation of an actual human, especially during fast walking. Figure A17 shows simulated RCS pattern of an adult male in running posture. It shows a slightly lower average RCS level and very different RCS pattern compared those in standing or walking postures.

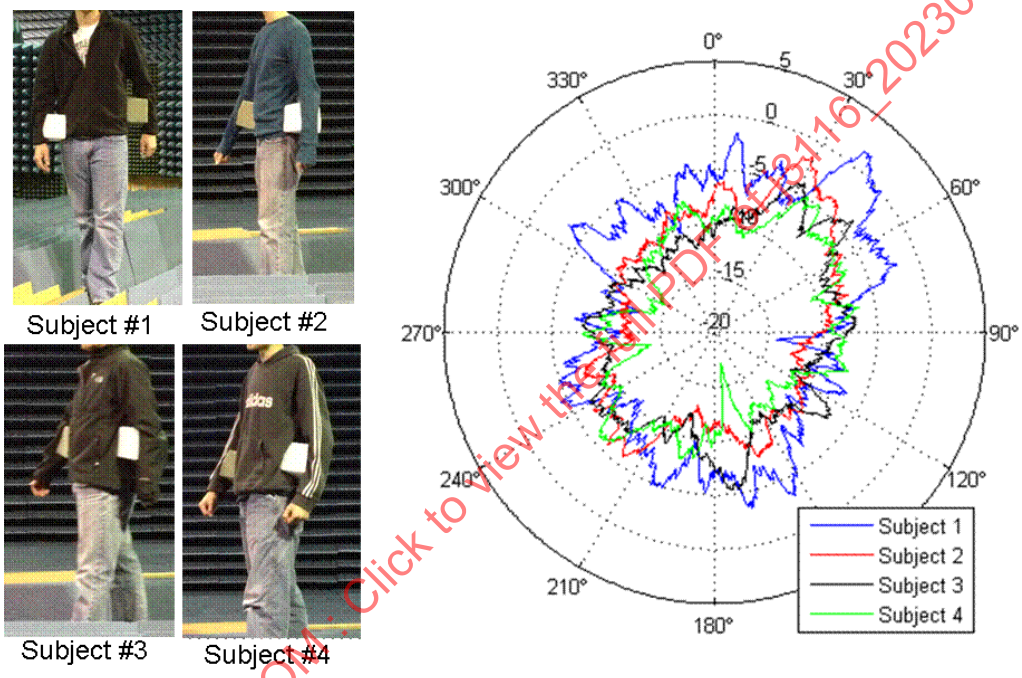

Figure A15 - Examples of smoothed RCS patterns of human subjects in walking postures

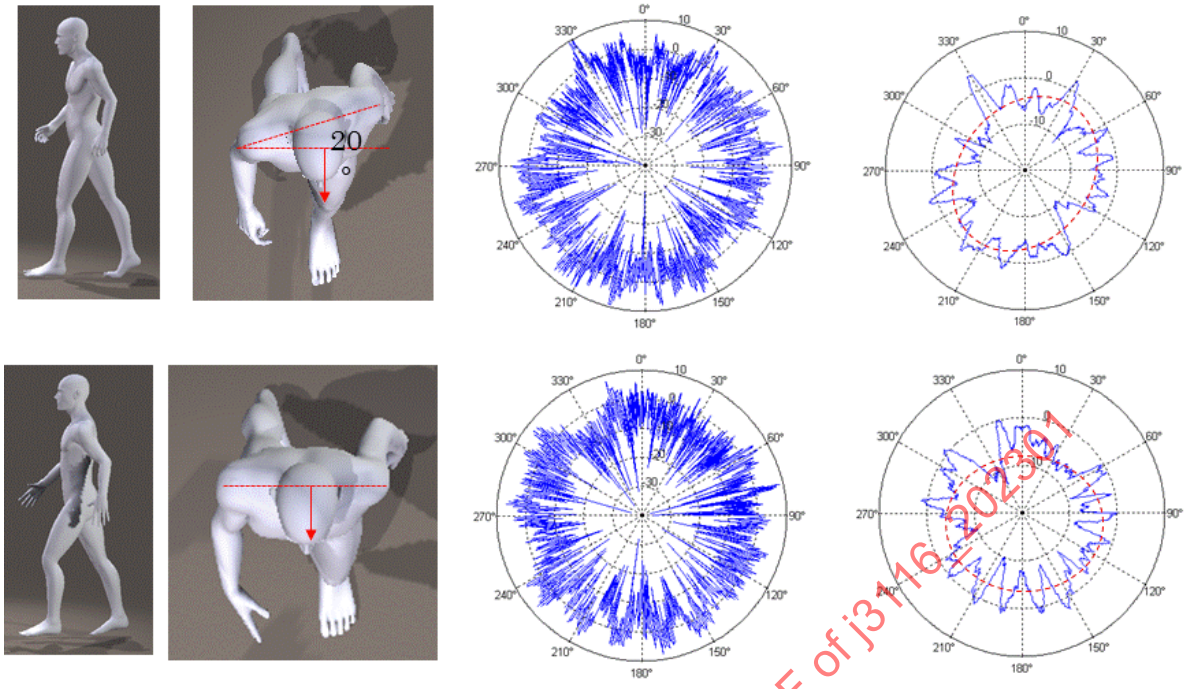

Figure A16 - Examples of smoothed RCS patterns of human subjects in walking postures

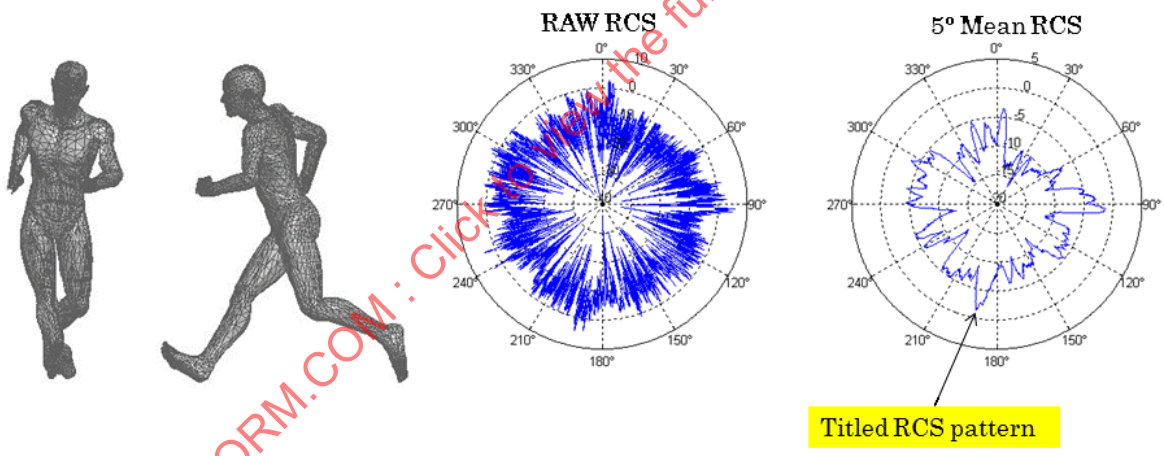

Figure A17 - Simulatted RCS patterns of a running adult male

A.5 CLOTHING EFFECT ON PEDESTRIAN RCS

In most cases, dry clothing made of light thin fabric has no effect on radar response of pedestrians in the 76 to 82 GHz frequency rang. This is demonstrated in Figure A18 where the moving-window standard deviation of RCS patterns and smoothed RCS patterns of a male subject dressed in short and T-shirt are compared with simulation results of undressed results obtained from a numerical model that was modeled after the human subject.

Figure A19 shows pictures of a male subject dressed in different seasonal clothing. The corresponding measured RCS STD patterns and 5° smoothed RCS patterns are compared in Figure A20. The RCS pattern data were collected from -10 to 190° in 0.2 steps. From these results, it is observed that:

- thicker clothing effectively increases the body's side-to-side width, and thus raising RCS level in the front and back directions, and
- thicker clothing also increasing the rotational symmetry, i.e., reducing the detail cross section contour variation, reducing RCS deviation.

Therefore, the clothing effect on pedestrian RCS is not significant except for special clothing materials or conditions such as clothes made of leather, clothes with excessive metal parts, or wet clothes.

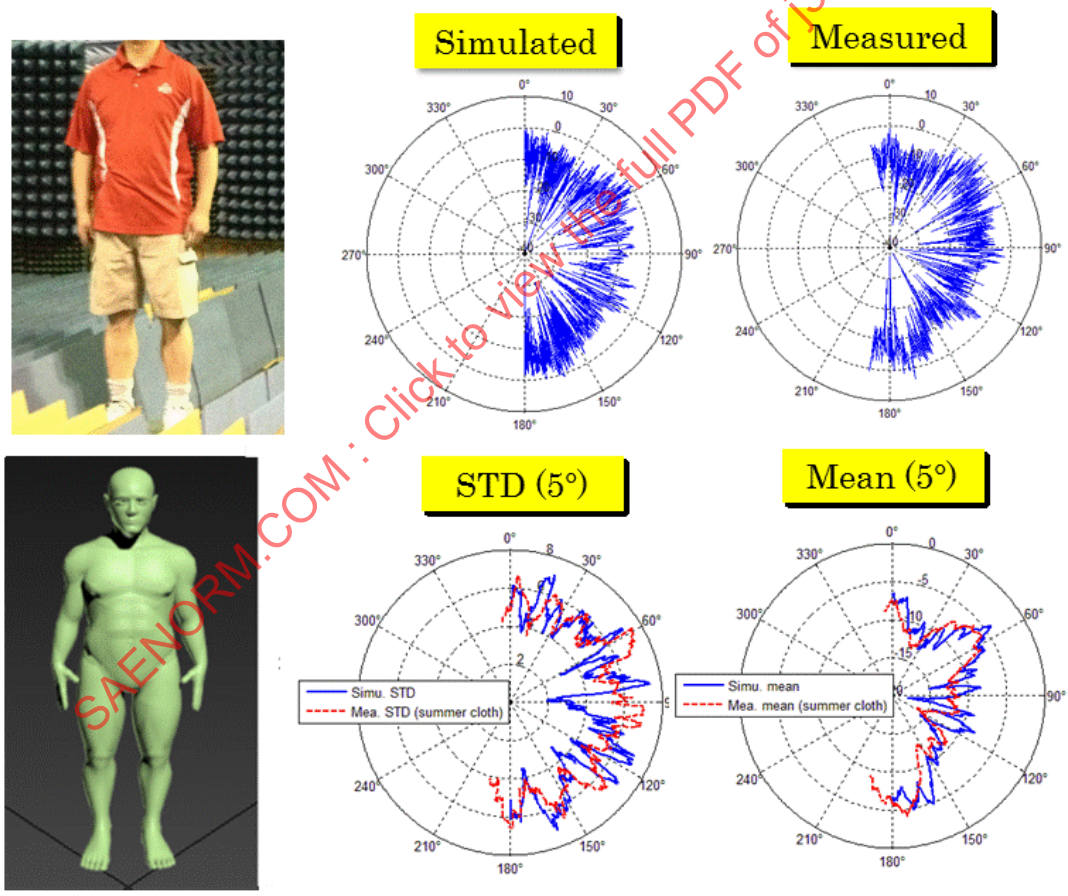

Figure A18 - Measured RCS pattern of lightly dressed human compared with simulated RCS patterns of naked human model that was modeled after the human subject